Physica D 36 (1989) 23–50
North-Holland, Amsterdam

COLLECTIVE DYNAMICS OF COUPLED OSCILLATORS WITH RANDOM PINNING

Steven H. STROGATZ[1,2], Charles M. MARCUS[2], Robert M. WESTERVELT[2] and Renato E. MIROLLO[3]
[1]*Department of Mathematics, Boston University, Boston, MA 02215, USA*
[2]*Division of Applied Sciences and Department of Physics, Harvard University, Cambridge, MA 02138, USA*
[3]*Department of Mathematics, Boston College, Chestnut Hill, MA 02167, USA*

Received 11 November 1988
Revised manuscript received 2 February 1989
Communicated by A.T. Winfree

We analyze a large system of nonlinear oscillators with random pinning, mean-field coupling and external drive. For small coupling and drive strength, the system evolves to an incoherent pinned state, with all the oscillators stuck at random phases. As the coupling or drive strength is increased beyond a depinning threshold, the steady-state solution switches to a coherent moving state, with all the oscillators moving nearly in phase. This depinning transition is discontinuous and hysteretic. We also show analytically that there is a delayed onset of coherence in response to a sudden superthreshold drive. The time delay increases as the threshold is approached from above. The discontinuous, hysteretic transition and the delayed onset of coherence are directly attributable to the form of the coupling, which is periodic in the phase difference between oscillators.

The system studied here provides a simple model of charge-density wave transport in certain quasi-one-dimensional metals and semiconductors in the regime where phase-slip is important; however this paper is intended primarily as a study of a model system with analytically tractable collective dynamics.

1. Introduction

Large systems of coupled nonlinear oscillators arise in many scientific contexts. They have been used to model cooperative dynamical systems in physics, chemistry, and biology, including charge-density waves [13, 15, 19, 40], oscillating chemical reactions [23, 44], and networks of oscillating nerve and heart cells [43, 44]. Coupled oscillators are also of great theoretical interest, as they provide tractable models for studies of nonlinear dynamics in systems with many degrees of freedom [1, 2, 4–9, 11–13, 22–25, 28, 30–40, 42–46].

1.1. *Model*

In this paper we analyze the following system of coupled oscillators in the infinite-N limit:

$$\dot{\theta}_i = E + b\sin(\alpha_i - \theta_i) + \frac{K}{N}\sum_{j=1}^{N}\sin(\theta_j - \theta_i), \quad i = 1,\ldots,N, \qquad (1.1)$$

where θ_i is the phase of the ith oscillator, $E, b, K \geq 0$ are fixed and the α_i are independent random variables uniformly distributed on $[0, 2\pi]$. The many-body system (1.1) provides a model of charge-density wave transport in certain quasi-one-dimensional metals and semiconductors, as discussed in section 1.5 and in [40]. Therefore we shall adopt some of the language used in the charge-density wave literature, giving definitions where appropriate.

The phases θ_i in (1.1) can be visualized as a swarm of points moving along the unit circle. The points move without inertia in response to three competing forces. The *pinning* term $b\sin(\alpha_i - \theta_i)$ tends to make θ_i stick at the random angle α_i. Hence this term favors a static, disordered arrangement of the phases θ_i. This pinning term is opposed by both the *applied field* E, which tends to drive the phases at a constant angular velocity and thus favors moving solutions; and by the *coupling* term $(K/N)\Sigma_j \sin(\theta_j - \theta_i)$, which tends to make $\theta_i = \theta_j$ and thus favors ordered solutions. The ratios K/b and E/b determine whether the

steady-state solutions of (1.1) are ordered or disordered, static or moving. Without loss of generality we normalize (1.1) by setting $b = 1$.

Roughly speaking one expects the following steady-state behavior of (1.1): for small E and K the pinning term dominates and the oscillators become pinned at random phases. As E increases with K fixed, the pinned state loses stability at some *depinning threshold* $E = E_T(K)$ and the system evolves to a steady-state moving solution.

Our goal is to characterize the steady-states and bifurcations of (1.1) as E and K are varied. In particular we will show that the depinning transition is *discontinuous*: the steady-state velocity of the moving solution jumps up discontinuously from zero at the depinning threshold. Furthermore the transition is *hysteretic*: if E is decreased, the moving solution does not re-pin until E falls below a separate pinning threshold E_P. Similar hysteretic and discontinuous transitions are seen experimentally in certain charge-density wave systems, as discussed in section 1.5.

1.2. *Organization of the paper*

In section 1.3 we outline our strategy for studying (1.1) analytically. The main idea is due to Kuramoto [22, 23, 25] and involves a dynamical version of self-consistent mean-field theory. Section 1.4 introduces the main phenomena exhibited by the model: switching, hysteresis, and delay. In section 1.5 we explain how the dynamical system (1.1) can be used to model charge-density wave transport in "switching samples." This section is introductory and assumes no prior knowledge about charge-density waves.

Sections 2–5 concern the mathematical analysis of (1.1). In section 2 we obtain all the static equilibrium solutions and analyze their bifurcations as the parameters E and K are varied. In section 3 we use variational methods to calculate the depinning threshold E_T, above which the pinned state loses stability and the system jumps to a moving solution.

Section 4 presents an analysis of the steady-state moving solutions. By seeking travelling-wave solutions of a form suggested by symmetry arguments, we reduce an infinite-dimensional problem to a boundary value problem for a single ordinary differential equation. Perturbation theory is used to obtain formal asymptotic solutions of this differential equation in two regimes: the high field limit $E \gg 1$ and the large coupling limit $K \gg 1$. Numerical simulations indicate that the moving solution disappears at a pinning threshold E_P; we argue that this disappearance occurs when a stable limit cycle corresponding to the moving solution coalesces with an unstable limit cycle.

Section 5 presents numerical and analytical results about delayed depinning in response to a sudden superthreshold drive. We derive an evolution equation for the phase coherence and use it to explain our numerical results.

Section 6 offers concluding remarks. We compare our work with previous studies and indicate some directions for future research.

In the appendix we present the details of the perturbation calculations needed in section 4.

1.3. *Infinite-range coupling*

A good starting point for analyzing a new many-body system is to assume that the coupling is infinite-range. This assumption usually simplifies the analysis while preserving many of the qualitative features found in models with nearest-neighbor or other kinds of short-range coupling. The infinite-range model (1.1) with $b = 1$ is

$$\dot{\theta}_i = E + \sin(\alpha_i - \theta_i) + \frac{K}{N}\sum_{j=1}^{N} \sin(\theta_j - \theta_i), \quad i = 1, \ldots, N, \qquad (1.2)$$

where the factor $1/N$ normalizes the coupling term. Because the sum extends over all j, (1.2) can be conveniently rewritten in terms of a mean-field

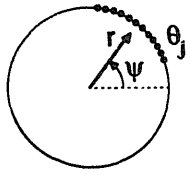

Fig. 1. The order parameter $re^{i\psi}$, as defined by (1.3). The radius r characterizes the coherence of the phases θ_j and the angle ψ characterizes the average phase. The collective velocity v is defined as $v = \dot{\psi}$.

quantity

$$re^{i\psi} = \frac{1}{N}\sum_{j=1}^{N} e^{i\theta_j} \tag{1.3}$$

to give

$$\dot{\theta}_i = E + \sin(\alpha_i - \theta_i) + Kr\sin(\psi - \theta_i), \quad i = 1,\ldots,N. \tag{1.4}$$

The quantity $re^{i\psi}$ provides an order parameter for the system [23, 25, 28, 40]. As shown in fig. 1, the magnitude r of the order parameter characterizes the amount of order or *coherence* in the configuration of the θ_j, and ψ defines the *average phase*. The quantity $v = \dot{\psi}$ measures the average velocity of the system.

At first glance (1.4) appears to be an uncoupled set of equations: $\dot{\theta}_i$ depends explicitly on θ_i, α_i, E, Kr and ψ, but not on the other θ_j. Of course θ_i *is* coupled to all the other θ_j, but only through the mean-field quantities r and ψ defined by (1.3). This observation led Kuramoto [22, 23, 25] to the following insight (in a different but related context): For finite N, one expects the coherence r and the average velocity v to vary in time. However for large N these variations should decrease as $\mathcal{O}(N^{-1/2})$. Hence to find the steady-state solutions of systems like (1.4) in the large N limit, one can impose a fixed r and v, solve (1.4) for all the $\theta_i(t)$, and then demand that the resulting solutions θ_i be consistent with (1.3) at all times. This requirement of *self-consistency* determines r and v and thus solves the problem.

In this paper we use this self-consistency argument to analyze the mean-field model (1.4) in the limit $N \to \infty$. The continuous analogue of (1.4) as $N \to \infty$ is

$$\dot{\theta}_\alpha = E + \sin(\alpha - \theta_\alpha) + Kr\sin(\psi - \theta_\alpha), \quad \alpha \in [0, 2\pi], \tag{1.5}$$

where the order parameter is now defined as

$$re^{i\psi} = \frac{1}{2\pi}\int_0^{2\pi} e^{i\theta_\alpha}\, d\alpha. \tag{1.6}$$

Note that a re-indexing has taken place between (1.4) and (1.5): because the equation of motion (1.4) depends on i only through α_i, we can re-label each θ in (1.5) by its associated α. This assumes that all oscillators with the same α eventually move identically, regardless of their initial conditions – this is certainly the case in our computer simulations.

1.4. *Switching, hysteresis, and delayed onset of coherence*

Eq. (1.5) can exhibit interesting dynamics because of its third term $Kr\sin(\psi - \theta_\alpha)$, which represents a collective force that pulls each θ_α towards the population average phase ψ. The collective force has an effective strength Kr that is proportional to the coherence r of the whole population. Thus an incoherent population exerts no force on any of its members. On the other hand, once coherence starts to develop, it can set off a *positive feedback* process: as r increases, the effective coupling Kr increases, thus tending to bring the phases closer together towards ψ, which makes r even larger, and so on. Whether this process becomes self-sustaining depends on the parameters K and E and on the initial conditions. For example, when $E = 0$ the static pinned configuration $\theta_\alpha = \alpha$ always solves (1.5): it has $r = 0$ so the collective pull vanishes, and the pinning forces $\sin(\alpha - \theta_\alpha)$ are also zero. But is this state stable? Clearly for K large enough the system is prone to

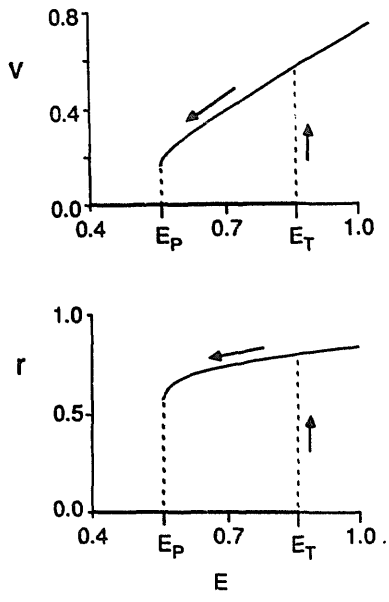

Fig. 2. Switching and hysteresis between pinned and moving solutions of (1.2). The velocity v and coherence r of the steady-state solutions of (1.2) are plotted against the applied field E. The data were obtained for $N = 300$ phases by numerical integration of (1.2) with $K = 1$. As E exceeds the depinning threshold E_T the system switches discontinuously from the incoherent pinned state ($r = 0$, $v = 0$) to the coherent moving state ($r > 0$, $v > 0$). As E is decreased the system switches back to the pinned state at a separate pinning threshold E_P. Because $E_P < E_T$, a hysteretic region is formed.

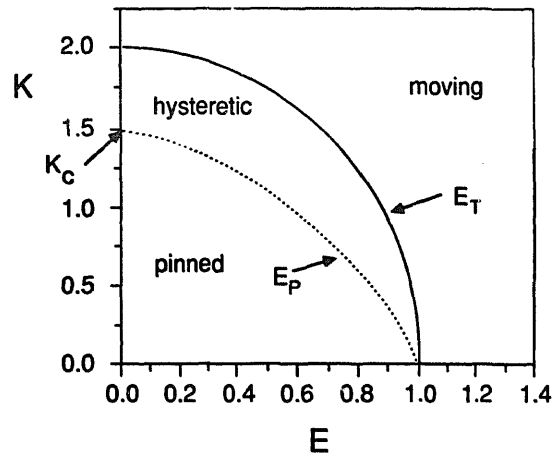

Fig. 3. Stability diagram for steady-state solutions of (1.2): solid line, depinning threshold $E_T = (1 - K^2/4)^{1/2}$ determined analytically in section 3; dashed line, pinning threshold E_P obtained by numerical integration of (1.2) for $N = 300$ phases.

the feedback process discussed above; it turns out that $K_T = 2$ is the threshold above which stability is lost (section 2.1) and the system jumps into a coherent configuration with $r \approx 1$.

We now present the results of numerical experiments which illustrate some of the behavior of (1.4) in the large N limit. For any initial conditions the infinite-N system always evolves to a steady-state solution for which the average velocity v and the coherence r are both time-independent. Fig. 2 plots the steady-state velocity and coherence of the system (1.4) against the applied field E for the case of $N = 300$ oscillators and coupling strength $K = 1$. For small E the system is pinned ($v = 0$) and incoherent ($r = 0$). When E exceeds the *depinning threshold* E_T, the velocity jumps up discontinuously, a phenomenon we call *switching* by analogy to the switching seen in the current–voltage characteristics of some charge-density wave systems [10, 15–21, 29, 41, 47]. With further increase in E, the velocity increases nearly linearly. If E is then decreased, the velocity decreases and then switches discontinuously to zero at the separate *pinning threshold* $E = E_P$ as shown in fig. 2(a). Fig. 2(b) shows that the coherence r of these solutions also exhibits *hysteresis* with discontinuous jumps at E_T and E_P.

The thresholds E_T and E_P depend on the coupling K, as shown by the bifurcation diagram plotted in fig. 3. The depinning threshold $E_T(K)$ is found analytically in section 3:

$$E_T(K) = \begin{cases} \sqrt{1 - \frac{K^2}{4}}, & K \le 2, \\ 0, & K > 2. \end{cases}$$

Note that for $K > 2$, the system moves for *any* $E > 0$. In other words the depinning threshold vanishes for sufficiently strong coupling. The pinning threshold E_P shown in fig. 3 was determined numerically using the initial condition $\theta_i = \theta_j \; \forall \, i, j$. We have not been able to derive an analytical expression for $E_P(K)$ when $E > 0$. The thresholds $E_T(K)$ and $E_P(K)$ in fig. 3 bound a hysteretic region where both pinned and moving solutions

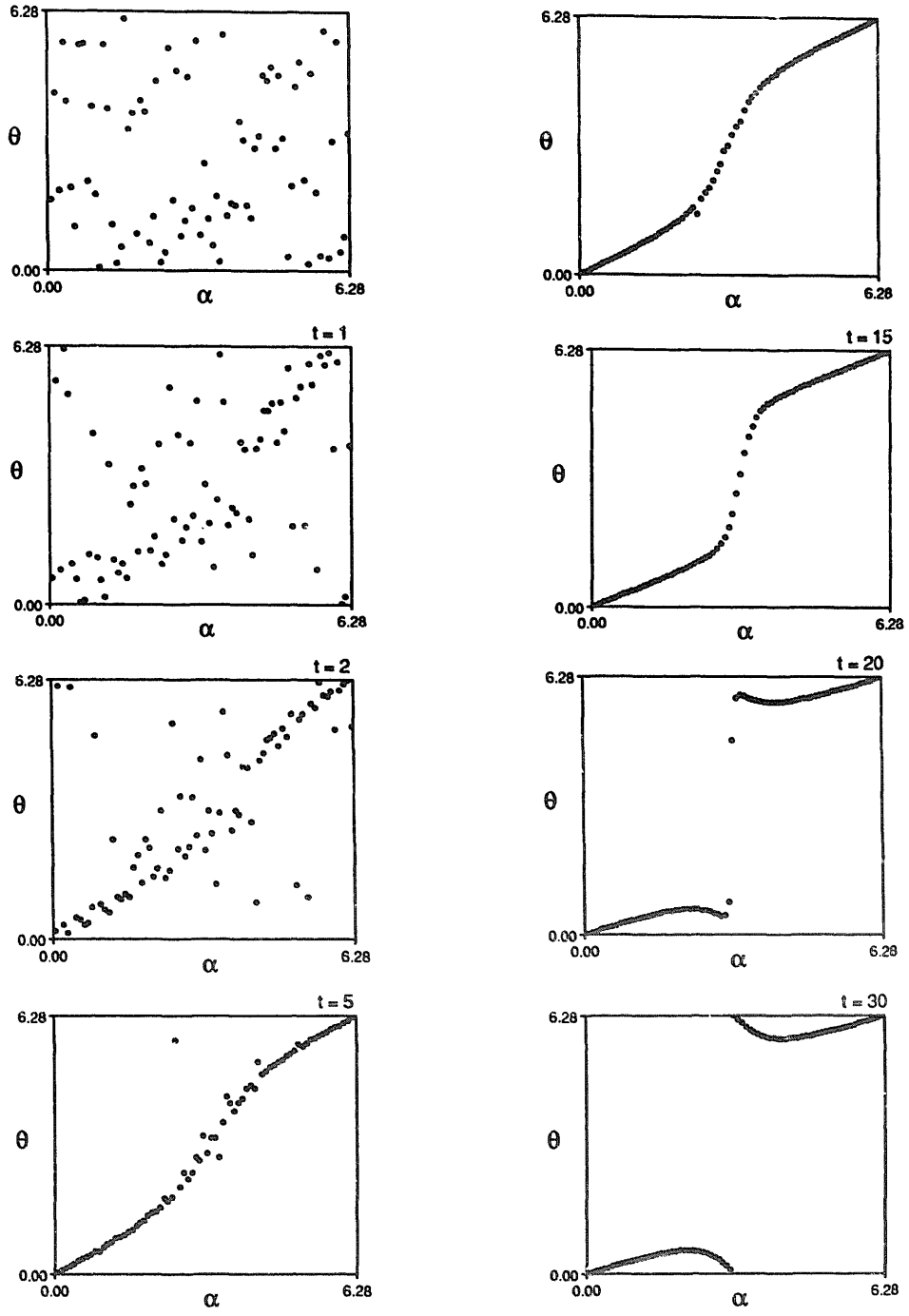

Fig. 4. Delayed onset of coherence for (1.2) when E and K are just above the depinning threshold and the initial state is incoherent. Eq. (1.2) was integrated numerically for $N = 300$ phases, with $E = 0$ and $K = 2.001$. For clarity, only every fourth phase is shown. The time corresponding to each panel is shown in its upper right hand corner. Starting from a random initial condition the system first evolves toward the diagonal, corresponding to the pinned state $\theta_i = \alpha_i$. The system slowly leaves the neighborhood of this saddle equilibrium, and eventually reaches the coherent final state by $t = 30$.

are stable; the final state reached depends on initial conditions.

The system (1.4) exhibits a peculiar transient behavior when the system is initially incoherent and when the parameters E and K are chosen just above the depinning threshold: before evolving to the globally attracting coherent state, the system approaches and lingers near a saddle equilibrium corresponding to the pinned state. This results in a *delayed onset of coherence*.

Fig. 4 shows the evolution of the phases θ_α starting from a random initial configuration, with $E = 0$ and $K = 2.001$. Note that the panels of fig. 4 are not equally spaced in time. The system first evolves rapidly toward the unstable pinned state $\theta_\alpha = \alpha$, corresponding to the diagonal in each panel of fig. 4. An unstable mode grows slowly and eventually leads to the ripping seen at $t = 20$. The coherent state is reached by $t = 30$. A theory of this delayed switching to the coherent state is presented in section 5.

1.5. *Charge-density wave transport*

Under certain conditions the behavior of charge-density waves can be modeled by the dynamical system presented in this paper. This section serves as an elementary introduction to charge-density wave transport for readers with no prior exposure to the subject. (For reviews see [15] or [19].) This section also discusses the strengths and weaknesses of our equations as a model of charge-density wave transport.

A charge-density wave is a collective electronic state found in certain quasi-one-dimensional metals and semiconductors. In these materials, a uniform distribution of conduction electrons loses stability below a critical temperature, giving rise to a periodic modulation of the charge density with an accompanying periodic distortion of the crystal lattice. Quasi-one-dimensional systems can be realized experimentally in materials which conduct current much more readily along one direction than along the other two.

Charge-density wave systems exhibit nonlinear conduction in response to an applied electric field: when the applied field is weak, the charge-density wave is pinned by impurities or defects in the lattice and carries no current; above a depinning threshold field E_T the charge-density wave breaks free from the pinning sites and slides through the crystal, carrying current.

Depinning of the charge-density wave can occur either continuously or discontinuously as the electric field is increased. Considerable theoretical attention has been given to the problem of continuous depinning [12–15, 19, 30, 37, 42] which characterizes the bulk of experimental data. On the other hand, systematic studies of discontinuous depinning, known as *switching*, have begun to appear only recently [10, 15–21, 29, 41, 47]. Switching is seen experimentally as a break in the current–voltage curve as the local electric field crosses E_T and the charge-density wave suddenly begins to move and carry current. Hysteresis frequently accompanies switching in these systems [18, 47]. That is, after the charge-density wave has depinned, it will not repin until the electric field is reduced well below E_T. Switching samples also exhibit a *delayed onset of nonlinear conduction* in response to a sudden super-threshold applied field [15, 19, 21, 47]. Switching is seen in charge-density wave systems with very strong pinning sites, created, for example, by radiation-induced defects [10, 16–21, 29, 41].

The charge density ρ in a one-dimensional charge-density wave system can be written as

$$\rho(x,t) = \rho_0 + \rho_{CDW}\cos(kx + \theta(x,t)), \qquad (1.7)$$

where $\theta(x,t)$ is the phase distortion of the charge-density wave at position x and time t. The charge-density wave has a preferred wavelength $\lambda = 2\pi/k$ but can be distorted (with some energy cost) to accommodate local impurities or defects in the lattice. When the pinning sites are very strong, the charge-density wave can be thought of as consisting of many coupled domains, each associated with one or several strong pinning sites.

Fig. 5 shows a schematic picture of a charge-density wave as a collection of domains, each with a well-defined phase – that is, the phase distortion $\theta(x, t)$ is a slowly varying function of x within a domain. Between domains, the amplitude ρ_{CDW} of the charge-density wave can collapse, allowing the phases of adjacent domains to advance at different rates [16–18, 20]. This phase-slip process relieves the energetically costly phase distortion at the expense of an amplitude collapse between domains.

The effects of pinning, elastic deformation and phase-slip are included in the following simple model [40] for the motion of each domain:

$$\dot{\theta}_i = E + b\sin(\alpha_i - \theta_i) + K\sum_j \sin(\theta_j - \theta_i), \quad i=1,\ldots,N. \tag{1.8}$$

Here θ_i is the phase distortion of the ith domain, E is the applied electric field, b is a typical pinning strength, α_i is the preferred random pinning phase for the ith domain, and K is the coupling strength between domains, which favors an undistorted wave. The periodic coupling term $\sin(\theta_j - \theta_i)$ is roughly linear for small phase difference $(\theta_j - \theta_i)$. Thus for small phase deformations this coupling corresponds to the elastic-coupling assumption used in previous treatments of charge-density wave dynamics [2, 12, 13, 30, 37, 42]. However the sinusoidal coupling also allows phase-slip between domains by giving a restoring force which softens and then reverses as the phase-difference $\theta_j - \theta_i$ increases.

This paper concerns the dynamics of (1.8) for the case of infinite-range coupling, and shows that the solutions of (1.8) exhibit switching, hysteresis, and delayed conduction. In this sense (1.8) provides a simple model of the nonlinear transport processes seen in charge-density wave switching samples.

However, in addition to the obviously unphysical assumption that all domains are coupled to each other with equal strength, there are several other limitations of (1.8) as a model of charge-density wave transport:

(1) Modelling phase-slip by a sinusoidal coupling term may capture some of the features of this complicated process, but is certainly not correct in detail. A more realistic model should include the amplitude of the charge-density wave as a dynamical variable. A model of switching in charge-density waves based on amplitude collapse at a single phase-slip center has been analyzed recently [16, 20].

(2) We have made the simplifying assumption that the coupling term in (1.8) is 2π-periodic in the phase difference $\theta_i - \theta_j$. This implies that phase-slip between neighboring domains will occur as soon as the phase difference between them exceeds π. In real charge-density wave systems a larger phase difference may be built up before a 2π phase-slip occurs [16, 20]. This has the important physical consequence that many energetically distinct metastable pinned states can exist; such states are observed experimentally [15, 19] but are not present in our model.

(3) The pinning strength b should be distributed across domains, rather than constant as we have assumed. This would allow different domains to depin at different applied fields, and may lead to multiple switching thresholds, an effect which has been observed experimentally [17, 18].

(4) The role of the "normal electrons" – those conduction electrons which are not condensed into the charge-density wave – has been completely neglected. The normal electrons provide an important parallel conduction path through the material and strongly influence the local electric fields felt by the charge-density wave domains.

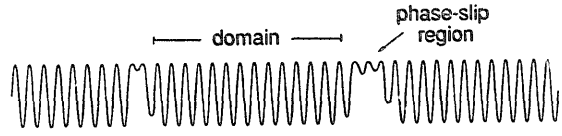

Fig. 5. Schematic representation of a charge-density wave undergoing phase-slip. Strong pinning sites separate the charge-density wave into domains. Between domains the amplitude of the charge-density wave can collapse allowing phase-slip.

2. Static solutions

In this section we consider static equilibrium solutions of the governing equations (1.5). The analysis divides naturally into two cases: $E = 0$ and $E > 0$.

The case $E = 0$ has been discussed in detail elsewhere [28] and will be reviewed only briefly here. The main result of this section is that there is a jump bifurcation in the coherence r when $K = K_c \approx 1.489$ and $K = K_T = 2$.

For $E > 0$, we show that a subcritical branch of static solutions with small r bifurcates along the depinning threshold $E_T = \sqrt{1 - K^2/4}$. All of these subcritical solutions are unstable, as can be shown by extending the methods of [28]. In section 2.2, we derive and analyze a self-consistent equation for the coherence $r = r(E, K)$ of these unstable static solutions and show that such solutions exist only if $E + Kr \leq 1$. We argue by contradiction: if static solutions exist for $E + Kr > 1$, then we obtain the contradiction that the coherence r or some of the phases θ_α must be complex.

Throughout this section, we emphasize that solutions with $r > 0$ arise as one-parameter families of configurations parametrized by the average phase ψ. This means that whenever there is one static solution to the equations, there is actually an entire *circle* of solutions in configuration space. This point is important to keep in mind; although it is obvious for the static case, it helps us to understand the moving solutions studied in later sections – the limit cycles studied there are seen here in degenerate form as circles of fixed points.

2.1. *Static solutions for* $E = 0$

2.1.1. *Explicit form of the solutions*

For $E = 0$ the solutions of (1.5) always evolve to a static equilibrium as $t \to \infty$. These static equilibria satisfy $\dot{\theta}_\alpha = 0$. Hence

$$0 = \sin(\alpha - \theta_\alpha) + Kr \sin(\psi - \theta_\alpha), \quad \alpha \in [0, 2\pi]. \tag{2.1}$$

Writing the sine functions as complex exponentials and solving (2.1) for the phases θ_α yields the equilibrium solution

$$e^{i\theta_\alpha} = e^{i\psi}\sqrt{\frac{Kr + e^{i(\alpha-\psi)}}{Kr + e^{-i(\alpha-\psi)}}} = e^{i\psi}\sqrt{\frac{u + e^{i\gamma}}{u + e^{-i\gamma}}}, \tag{2.2}$$

where

$$u = Kr \tag{2.3}$$

and

$$\gamma = \alpha - \psi. \tag{2.4}$$

Thus for each u, there is a one-parameter family of configurations (2.2) parametrized by ψ.

2.1.2. *Self-consistency equation*

The solution (2.2) must be consistent with the definition of the order parameter: $re^{i\psi} = (1/2\pi)\int_0^{2\pi} e^{i\theta_\alpha} d\alpha$. Hence

$$re^{i\psi} = \frac{1}{2\pi}\int_0^{2\pi} e^{i\psi}\left(\frac{u + e^{i\gamma}}{u + e^{-i\gamma}}\right)^{1/2} d\gamma. \tag{2.5}$$

Note that the factor $e^{i\psi}$ cancels from (2.5). Thus ψ is arbitrary, reflecting the rotational symmetry in the system. From (2.5) we obtain the self-consistency equation for r:

$$r = f(u), \tag{2.6}$$

where

$$f(u) = \frac{1}{2\pi}\int_0^{2\pi}\left(\frac{u + e^{i\gamma}}{u + e^{-i\gamma}}\right)^{1/2} d\gamma = \frac{1}{2\pi}\int_0^{2\pi}\frac{u + \cos\gamma}{\sqrt{1 + 2u\cos\gamma + u^2}}\, d\gamma. \tag{2.7}$$

The function $f(u)$ may be expressed exactly in terms of elliptic integrals [28].

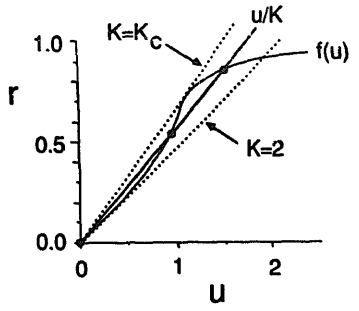

Fig. 6. Solution of the self-consistency equations (2.6) and (2.7). Solid lines indicate the integral $f(u)$ plotted from (2.7) together with the line u/K (see text). Equilibrium solutions for r occur where $f(u)$ intersects the line u/K. For the values of K shown, three solutions exist (filled circles). Dashed lines show u/K for the bifurcation values $K = K_c$ and $K = K_T = 2$.

Fig. 6 shows the graph of $f(u)$. At fixed K, the corresponding values of r are found at the intersections of the curve $r = f(u)$ with the line $r = u/K$ (fig. 6). Note that jump bifurcations occur where the line intersects the curve tangentially, at $K = K_c \approx 1.489$ and $K = K_T = 2$. The resulting curve of of r versus K is plotted in fig. 7.

2.1.3. *Stability of the solutions*

In [28] we prove the following results about stability:

(i) When $r = 0$, the incoherent pinned solution $\theta_\alpha = \alpha$ is globally stable for $K < K_c$, locally stable for $K < 2$ and unstable for $K > 2$. All other solutions with $r = 0$ are unstable.

(ii) For each $u > 0$, there is a one-parameter family or "circle" of static solutions (2.2) parametrized by ψ.

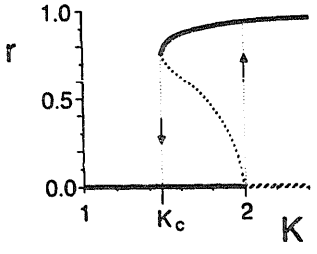

Fig. 7. Coherence r of the static equilibrium solutions of (1.5) with $E = 0$, plotted against the normalized coupling strength K. Solid lines, locally stable equilibria; broken lines, unstable equilibria. Jump bifurcations occur at $K = K_c$ and $K = 2$.

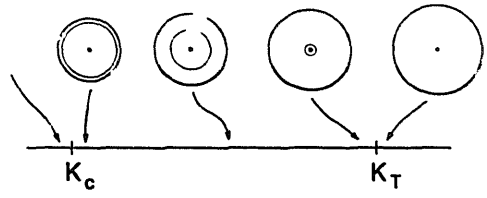

Fig. 8. Schematic bifurcation diagram for equilibrium of (1.5) with $E = 0$. The coherence r and the average phase ψ of the equilibria are plotted in polar coordinates. The origin $r = 0$ corresponds to the pinned state $\theta_\alpha = \alpha$, which is locally stable for $K < K_T$. A circle of saddle equilibria (thin line) and a circle of stable equilibria (thick line) appear at large r when $K = K_c$. The pinned state $\theta_\alpha = \alpha$ loses stability at $K = K_T$ when it coalesces with the circle of saddle points. Above K_T the only attractor is the circle of stable points with large coherence.

(iii) For $u > u_c \approx 1.100$, the critical circle is locally stable to perturbations in all directions transverse to the circle. For $u < u_c$, the critical circle consists of saddle points which are unstable in precisely one direction. For all u, the critical points are neutrally stable to motion along the circle in the ψ direction.

(iv) The circle of saddles coalesces with the circle of stable points at $K = K_c$. As $K \to K_T = 2$, $u \to 0$, the saddle configurations for different ψ become more and more alike, and the "radius" of the circle shrinks. At $K = K_T$ a saddle circle coalesces with the incoherent pinned state.

2.1.4. *Schematic bifurcation diagram*

Fig. 8 illustrates the transitions discussed above. The diagram is familiar from the Landau theory of first-order phase transitions or the theory of subcritical Hopf bifurcations. For each equilibrium configuration θ_α given by (2.2), the average phase ψ is plotted as the polar angle, and the coherence r as the radius. A circle of stable points with large r coalesces with a circle of unstable points at $K = K_c$, and both are annihilated for $K < K_c$. A small circle of unstable points coalesces with the stable $r = 0$ configuration at $K = K_T$, rendering it unstable for $K > K_T$.

Fig. 8 is very schematic because each point actually represents a configuration θ_α, $\alpha \in [0, 2\pi]$, and therefore belongs to an *infinite*-dimensional

function space, not a two-dimensional space. However, the picture is qualitatively faithful: as shown by (2.2) there is a two-parameter family of equilibria for (2.1), parametrized by the average phase ψ and by $u = Kr$; the *topological* aspects of the bifurcation are captured correctly by our two-dimensional representation.

2.2. *Static solutions for* $E > 0$

In this section we compute the shape and coherence of the static configurations for $E > 0$, and show that they exist only if $E + Kr \leq 1$.

2.2.1. *Explicit form of the solutions*

The static solutions now satisfy the equation

$$\dot{\theta} = E + \sin(\alpha - \theta_\alpha) + Kr\sin(\psi - \theta_\alpha), \quad \alpha \in [0, 2\pi]. \tag{2.8}$$

For $r = 0$, there are two self-consistent continuous solutions of (2.8):

$$\theta_\alpha = \alpha + \sin^{-1} E \tag{2.9}$$

and

$$\theta_\alpha = \alpha + \pi + \sin^{-1} E \tag{2.10}$$

where $\sin^{-1} E \in [-\pi/2, \pi/2]$.

The stability of the solution (2.9) will be analyzed in section 3, where it is shown that (2.9) is locally stable if and only if $E < E_T(K) = (1 - K^2/4)^{1/2}$. The same analysis shows that (2.10) is *always* unstable.

For $r > 0$, there is one-parameter family of solutions of (2.8) for fixed E and K, parametrized by the average phase ψ. Without loss of generality, we restrict our attention from now on to solutions with

$$\psi = 0. \tag{2.11}$$

(To obtain all other solutions, replace θ_α and α by $\theta_\alpha - \psi$ and $\alpha - \psi$ respectively.)

Solving (2.8) with complex exponentials we obtain

$$e^{i\theta_\alpha} = \frac{iE \pm \sqrt{|u + e^{i\alpha}|^2 - E^2}}{u + e^{-i\alpha}}, \quad \alpha \in [0, 2\pi], \tag{2.12}$$

where $u = Kr$.

2.2.2. *Existence conditions*

Eq. (2.12) must be consistent with (2.11) and with

$$r = \frac{1}{2\pi}\int_0^{2\pi} e^{i\theta_\alpha}\, d\alpha, \quad r \geq 0. \tag{2.13}$$

In particular r must be real. Also we require that θ_α be real for all α.

We show now that these reality constraints are satisfied if and only if $u + E \leq 1$, where $u, E > 0$. First we rewrite (2.12) in a simpler form. We define ρ and σ by

$$\rho e^{i\sigma} = u + e^{i\alpha}, \quad \rho(u, \alpha) \geq 0; \quad \sigma(u, \alpha) \in [0, 2\pi]. \tag{2.14}$$

In terms of ρ and σ, (2.12) becomes

$$e^{i\theta_\alpha} = \frac{iE \pm \sqrt{\rho^2 - E^2}}{\rho e^{-i\sigma}} = e^{i\sigma}\left(i\frac{E}{\rho} \pm \sqrt{1 - \left(\frac{E}{\rho}\right)^2}\right). \tag{2.15}$$

Because we want (2.15) to branch from the stable solution for $E = 0$, we take the solution (2.15) in which the square root is *added* to iE/ρ. Then making the change of variables

$$\sin\chi = E/\rho, \quad \cos\chi = \sqrt{1 - \left(\frac{E}{\rho}\right)^2}, \tag{2.16}$$

we obtain $e^{i\theta_\alpha} = e^{i\sigma}e^{i\chi}$ or

$$\vartheta_\alpha = \sigma + \chi, \quad \alpha \in [0, 2\pi]. \tag{2.17}$$

Since $\sigma(u, \alpha)$ and θ_α are real for all α, then $\chi = \chi(E, \rho(u, \alpha))$ must also be real for all α. From (2.16) this condition reduces to

$$E \le \min_\alpha \rho(u, \alpha) = |1 - u|. \tag{2.18}$$

From (2.12) and (2.13) the self-consistency equation for r is

$$r = \frac{1}{2\pi}\int_0^{2\pi} \frac{iE + \sqrt{|u + e^{i\alpha}|^2 - E^2}}{u + e^{-i\alpha}}\, d\alpha. \tag{2.19}$$

The integral (2.19) splits into two pieces. The first piece is

$$\frac{1}{2\pi}\int_0^{2\pi} \frac{iE}{u + e^{-i\alpha}}\, d\alpha = \frac{E}{u}\frac{1}{2\pi}\int_0^{2\pi} \frac{e^{i\alpha} d\alpha}{u^{-1} + e^{i\alpha}} = \frac{E}{u}\frac{1}{2\pi}\int_{|z|=1} \frac{dz}{z + u^{-1}} = \begin{cases} 0, & u < 1, \\ iE/2u, & u = 1, \\ iE/u, & u > 1. \end{cases} \tag{2.20}$$

The second piece of the integral (2.19) is real. To see this, let

$$g(\alpha) = \frac{\sqrt{|u + e^{i\alpha}|^2 - E^2}}{u + e^{-i\alpha}}. \tag{2.21}$$

Because of (2.18) the numerator in (2.21) is real for all α. Therefore

$$g^*(\alpha) = g(-\alpha)\ \forall \alpha, \tag{2.22}$$

where the star denotes complex conjugation. Thus the integral of g is real:

$$\int_0^{2\pi} g(\alpha)\, d\alpha = \int_0^{\pi} [g(\alpha) + g(-\alpha)]\, d\alpha = \int_0^{\pi} [g(\alpha) + g^*(\alpha)]\, d\alpha = \mathrm{Re}\left[2\int_0^{\pi} g(\alpha)\, d\alpha\right]. \tag{2.23}$$

Combining (2.20) and (2.23) we conclude that

$$u < 1 \tag{2.24}$$

is required for the integral in (2.19) to be real. Now (2.18) implies the stronger inequality $E \le 1 - u$ or

$$u + E \le 1. \tag{2.25}$$

The upshot is that condition (2.25) is necessary and sufficient for the existence of static solutions for $E > 0$. (For $E = 0$, the argument fails – as it must – because the integral in (2.20) vanishes.)

2.2.3. *Self-consistency equation*

In this section we derive the self-consistency equation for the coherence r of the static solutions (2.12). By expanding this equation in powers of $u = Kr$ we show that these solutions branch off from the $r = 0$ pinned solution along the curve $E^2 + K^2/4 = 1$. It is also shown that this branch is subcritical in the sense that it exists only for E below threshold E_T, where

$$E_T = \sqrt{1 - K^2/4}.$$

The self-consistency equation is

$$\frac{u}{K} = r$$
$$= \frac{1}{2\pi}\int_0^{2\pi} \frac{iE + \sqrt{|u+e^{i\alpha}|^2 - E^2}}{u+e^{-i\alpha}}\,d\alpha$$
$$= \frac{1}{2\pi}\int_0^{2\pi} \frac{\sqrt{1-E^2+2u\cos\alpha+u^2}}{1+2u\cos\alpha+u^2} \times (u+\cos\alpha)\,d\alpha, \qquad (2.26)$$

where the imaginary part of the integral vanishes as in (2.20) because we are assuming that $u + E \leq 1$.

Note that $u = 0$ solves (2.26) for all $E, K > 0$. To find when solutions with small $u > 0$ bifurcate from this trivial solution, we expand (2.26) in powers of $u \ll 1$. After evaluating the resulting integrals we obtain

$$\frac{u}{K} = \frac{u}{2\sqrt{1-E^2}}\left[1 + \frac{u^2}{8}\,\frac{1+2E^2}{(1-E^2)^2} + \mathcal{O}(u^4)\right]. \qquad (2.27)$$

Thus non-trivial solutions branch from $u = 0$ along the curve $K = 2\sqrt{1-E^2}$. For fixed E, let

$$K_T = 2\sqrt{1-E^2}. \qquad (2.28)$$

As $K \to K_T$ from below, the static solutions satisfy

$$\frac{K_T}{K} = 1 + \frac{u^2}{8}\,\frac{1+2E^2}{(1+E^2)^2} + \mathcal{O}(u^4), \qquad (2.29)$$

which implies the subcritical behavior

$$r \sim \left[\frac{(1-E^2)^{1/4}}{(1+2E^2)^{1/2}}\right]\sqrt{K_T - K}. \qquad (2.30)$$

Note that the term in brackets tends to zero (but very slowly) as $E \to 1^-$.

2.2.4. *Static configurations for* $0 < r \ll 1$

As $E \to E_T$, a branch of *static subcritical solutions* with small positive r approaches the incoherent ($r = 0$) solution $\theta_\alpha = \alpha + \sin^{-1} E$. In fact, an entire *circle* of subcritical solutions parametrized by ψ coalesces with the incoherent state at $E = E_T$. In this section we calculate the shape of those subcritical solutions to leading order as $r \to 0$. As before, we restrict attention to the case $\psi = 0$ without loss of generality. From (2.17) we have $\theta_\alpha = \sigma + \chi$. We first find σ to $\mathcal{O}(u)$ as follows. Eq. (2.14) implies

$$e^{i\sigma} = \frac{u+e^{i\alpha}}{|u+e^{i\alpha}|}$$
$$= \sqrt{\frac{u+e^{i\alpha}}{u+e^{-i\alpha}}}$$
$$= e^{i\alpha}(1 - iu\sin\alpha + \mathcal{O}(u^2))$$
$$= e^{i\alpha}e^{-iu\sin\alpha} + \mathcal{O}(u^2), \qquad (2.31)$$

so

$$\sigma = \alpha - u\sin\alpha + \mathcal{O}(u^2). \qquad (2.32)$$

To find χ to $\mathcal{O}(u)$ we recall

$$\sin\chi = E/\rho$$
$$= E/\sqrt{1+2u\cos\alpha+u^2}$$
$$= E(1-u\cos\alpha) + \mathcal{O}(u^2), \qquad (2.33)$$

which can be inverted to yield

$$\chi = \sin^{-1} E - \frac{uE\cos\alpha}{\sqrt{1-E^2}} + \mathcal{O}(u^2). \qquad (2.34)$$

Hence

$$\theta_\alpha = \sigma + \chi$$
$$= \alpha + \sin^{-1} E - u\left[\sin\alpha + \frac{E\cos\alpha}{\sqrt{1-E^2}}\right] + \mathcal{O}(u^2). \qquad (2.35)$$

It is significant that the leading order corrections lie in the subspace of configurations spanned by $\{\sin\alpha, \cos\alpha\}$; as will be seen in section 3, these are precisely the modes which lose stability at the depinning threshold E_T.

3. Depinning threshold E_T

In this section we analyze the local stability of the incoherent pinned solution $\theta_\alpha = \alpha + \sin^{-1} E$. We show that this solution is a local minimum of the potential function if and only if $E < E_T(K) = \sqrt{1 - K^2/4}$. We also find that for $E > E_T$ the pinned state is unstable to small perturbations of the form $\eta(\alpha) = a\sin\alpha + b\cos\alpha$.

In the presence of an applied field E, the governing equations are

$$\dot\theta_\alpha = E + \sin(\alpha - \theta_\alpha) + Kr\sin(\psi - \theta_\alpha), \quad \alpha \in [0, 2\pi], \tag{3.1}$$

$$re^{i\psi} = \frac{1}{2\pi}\int_0^{2\pi} e^{i\theta_\alpha}\,d\alpha. \tag{3.2}$$

There is a solution of these equations which is pinned ($\dot\theta_\alpha = 0\ \forall\alpha$) and incoherent ($r = 0$). Such a solution satisfies $E + \sin(\alpha - \theta_\alpha) = 0$ or

$$\theta_\alpha = \alpha + \sin^{-1} E, \quad \alpha \in [0, 2\pi]. \tag{3.3}$$

Note that this solution exists for all $|E| \le 1$. The configuration (3.3) is a rotated version of the pinned solution $\theta_\alpha = \alpha$ found earlier for $E = 0$. To recover the stable solution found when $E = 0$, we want the branch of the inverse sine that satisfies $\cos(\sin^{-1} E) \ge 0$.

We now analyze the local stability of the pinned state (3.3) by diagonalizing the second variation of the system's potential function about that state. This potential function H satisfies

$$\dot\theta_\alpha = -\frac{\delta H}{\delta\theta_\alpha}, \tag{3.4}$$

where

$$H(\theta_\alpha) = -E\int_0^{2\pi}\theta_\alpha\,d\alpha - \int_0^{2\pi}\cos(\alpha - \theta_\alpha)\,d\alpha - \frac{K}{4\pi}\int_0^{2\pi}\int_0^{2\pi}\cos(\theta_\beta - \theta_\alpha)\,d\alpha\,d\beta. \tag{3.5}$$

Let $\theta_\alpha(\epsilon)$ denote a small variation about the static solution (3.3):

$$\theta_\alpha(\epsilon) = \alpha + \sin^{-1} E + \epsilon\eta_\alpha, \tag{3.6}$$

where $\epsilon \ll 1$ and η: $\alpha \mapsto \eta_\alpha$ is a perturbation. For fixed η, H is a function of the single variable ϵ. We are particularly interested in the second variation Γ given by

$$\Gamma = \frac{d^2}{d\epsilon^2} H(\theta_\alpha(\epsilon))\bigg|_{\epsilon=0} \tag{3.7}$$

because it determines the local stability of (3.3). Recall that the second variation is a quadratic form in η; if Γ is positive definite, i.e., $\Gamma(\eta) > 0\ \forall\,\eta \ne 0$, then the configuration (3.3) is a local minimum of H and is therefore locally stable.

To calculate Γ we first substitute (3.6) into (3.5) which yields

$$H = -E\int_0^{2\pi}(\alpha + \sin^{-1} E + \epsilon\eta_\alpha)\,d\alpha - \int_0^{2\pi}\cos(\epsilon\eta_\alpha + \sin^{-1} E)\,d\alpha - \frac{K}{4\pi}\int_0^{2\pi}\int_0^{2\pi}\cos(\beta - \alpha + \epsilon\eta_\beta - \epsilon\eta_\alpha)\,d\alpha\,d\beta. \tag{3.8}$$

Hence

$$\frac{dH}{d\epsilon} = -E\int_0^{2\pi}\eta_\alpha\,d\alpha + \int_0^{2\pi}\eta_\alpha \times\sin\left(\epsilon\eta_\alpha + \sin^{-1}E\right)d\alpha + \frac{K}{4\pi}\int_0^{2\pi}\int_0^{2\pi}(\eta_\beta-\eta_\alpha) \times\sin\left(\beta-\alpha+\epsilon\eta_\beta-\epsilon\eta_\alpha\right)d\alpha\,d\beta, \tag{3.9}$$

and

$$\frac{d^2H}{d\epsilon^2} = \int_0^{2\pi}\eta_\alpha^2\cos\left(\epsilon\eta_\alpha+\sin^{-1}E\right)d\alpha + \frac{K}{4\pi}\int_0^{2\pi}\int_0^{2\pi}(\eta_\beta-\eta_\alpha)^2 \times\cos\left(\beta-\alpha+\epsilon\eta_\beta-\epsilon\eta_\alpha\right)d\alpha\,d\beta. \tag{3.10}$$

To find Γ we evaluate (3.10) at $\epsilon = 0$. Thus

$$\Gamma(\eta) = \sqrt{1-E^2}\int_0^{2\pi}\eta_\alpha^2\,d\alpha + \frac{K}{4\pi}\int_0^{2\pi}\int_0^{2\pi}(\eta_\beta-\eta_\alpha)^2\cos(\beta-\alpha)\,d\alpha\,d\beta. \tag{3.11}$$

The second integral on the right side of (3.11) may be simplified in two steps. First, when we expand the term $(\eta_\beta-\eta_\alpha)^2$, only the integral involving $\eta_\alpha\eta_\beta$ survives – the others integrate to zero. Hence

$$\int_0^{2\pi}\int_0^{2\pi}(\eta_\beta-\eta_\alpha)^2\cos(\beta-\alpha)\,d\alpha\,d\beta = -2\int_0^{2\pi}\int_0^{2\pi}\eta_\alpha\eta_\beta\cos(\beta-\alpha)\,d\alpha\,d\beta. \tag{3.12}$$

Second, we expand the term $\cos(\beta-\alpha)$ on the right side of (3.12) and note that the α and β integrals separate, conveniently yielding a Fourier transform:

$$\begin{aligned}\int_0^{2\pi}\int_0^{2\pi}\eta_\alpha\eta_\beta\cos(\beta-\alpha)\,d\alpha\,d\beta &= \int_0^{2\pi}\int_0^{2\pi}\eta_\alpha\eta_\beta(\cos\alpha\cos\beta+\sin\alpha\sin\beta)\,d\alpha\,d\beta\\ &= \left[\int_0^{2\pi}\eta_\alpha\cos\alpha\,d\alpha\right]^2+\left[\int_0^{2\pi}\eta_\alpha\sin\alpha\,d\alpha\right]^2\\ &= \left|\int_0^{2\pi}\eta_\alpha e^{i\alpha}d\alpha\right|^2\\ &= 4\pi^2|\hat\eta(-1)|^2,\end{aligned} \tag{3.13}$$

where the Fourier transform $\hat\eta$ is defined by

$$\hat\eta(k) = \frac{1}{2\pi}\int_0^{2\pi}\eta_\alpha e^{-ik\alpha}d\alpha. \tag{3.14}$$

The upshot is that (3.11) may be rewritten as

$$\begin{aligned}\Gamma(\eta) &= \sqrt{1-E^2}\int_0^{2\pi}\eta_\alpha^2\,d\alpha - 2\pi K|\hat\eta(-1)|^2\\ &= 2\pi\left[\sqrt{1-E^2}\|\eta\|^2 - K|\hat\eta(-1)|^2\right],\end{aligned} \tag{3.15}$$

where

$$\|\eta\|^2 = \frac{1}{2\pi}\int_0^{2\pi}\eta_\alpha^2\,d\alpha. \tag{3.16}$$

The quadratic form (3.15) can be diagonalized as follows. We work in the Hilbert space $L^2(S^1)$ of square integrable functions with the inner product

$$\mu\cdot\nu = \frac{1}{2\pi}\int_0^{2\pi}\mu_\alpha\nu_\alpha\,d\alpha. \tag{3.17}$$

Let

$$\mu_\alpha = \cos\alpha, \quad \nu_\alpha = \sin\alpha. \tag{3.18}$$

Then $\|\mu\|^2 = \|\nu\|^2 = \frac{1}{2}$ and $\mu \cdot \nu = 0$. Write η in an orthogonal decomposition using μ and ν:

$$\eta_\alpha = a\frac{\mu_\alpha}{\|\mu\|} + b\frac{\nu_\alpha}{\|\nu\|} + \eta_\alpha^\perp, \tag{3.19}$$

where $\mu \cdot \eta^\perp = \nu \cdot \eta^\perp = 0$. That is, we express η as a linear combination of μ, ν, and some function $\eta^\perp$ orthogonal to both μ and ν.

Then

$$\|\eta\|^2 = a^2 + b^2 + \|\eta^\perp\|^2 \tag{3.20}$$

and

$$\begin{aligned}
|\hat{\eta}(-1)|^2 &= \left(\frac{1}{2\pi}\int_0^{2\pi} \eta_\alpha \cos\alpha \, d\alpha\right)^2 + \left(\frac{1}{2\pi}\int_0^{2\pi} \eta_\alpha \sin\alpha \, d\alpha\right)^2 \\
&= (\eta \cdot \mu)^2 + (\eta \cdot \nu)^2 \\
&= (a\|\mu\|)^2 + (b\|\nu\|)^2 \\
&= \frac{a^2 + b^2}{2}.
\end{aligned} \tag{3.21}$$

Thus (3.15) has been diagonalized to the form

$$\begin{aligned}
\frac{1}{2\pi}\Gamma(\eta) &= \sqrt{1 - E^2}\,(a^2 + b^2 + \|\eta^\perp\|^2) - K\left(\frac{a^2 + b^2}{2}\right) \\
&= (a^2 + b^2)\left(\sqrt{1 - E^2} - \frac{K}{2}\right) + \sqrt{1 - E^2}\,\|\eta^\perp\|^2.
\end{aligned} \tag{3.22}$$

Eq. (3.22) expresses Γ as the sum of two forms: $\|\eta^\perp\|^2$ is positive definite, and the form containing $a^2 + b^2$ is positive, zero, or negative depending on the quantity $\sqrt{1 - E^2} - K/2$. In particular, Γ is itive definite if and only if $\sqrt{1 - E^2} - K/2 > 0$. Hence the incoherent pinned state (3.3) loses stability at the depinning threshold given by

$$E_T = \sqrt{1 - \frac{K^2}{4}}. \tag{3.23}$$

Note that at $E = E_T$ the unstable subcritical solutions (3.12) coalesce with the incoherent state (3.3), as shown in section 2.2.3.

The present analysis also reveals the instability modes. For $E > E_T$, the incoherent state (3.3) is unstable to any perturbation of the form

$$\begin{aligned}
\eta_\alpha &= a\mu_\alpha + b\nu_\alpha \\
&= a\cos\alpha + b\sin\alpha,
\end{aligned} \tag{3.24}$$

which is a linear combination of eigenfunctions (3.18). To leading order in r, this is precisely the form of the subcritical solutions (2.35) as they approach the $r = 0$ state (3.3). In terms of Fourier series, the first harmonic of θ_α is unstable, while all higher harmonics are stable. This instability of the first harmonic is strikingly apparent in fig. 4, between $t = 5$ and $t = 20$.

4. Moving solutions

In this section we analyze the steady-state moving solutions of (1.5). In section 4.1 we seek travelling-wave solutions of a certain form motivated by symmetry arguments and the results of computer simulations. This *ansatz* reduces the original infinite-dimensional dynamical system to an ordinary differential equation in one variable, subject to three side conditions. Sections 4.2 and 4.3 use regular perturbation theory to approximate the wave-shape, coherence, and velocity of the stable moving solution for large E (section 4.2) and large K (section 4.3).

Numerical results indicate that steady-state moving solutions exist if and only if E exceeds the pinning threshold $E_P(K)$. Section 4.4 discusses the bifurcation that occurs at $E = E_P$. We conjecture that the stable moving solution, which corresponds to a stable limit cycle in configuration space, ceases to exist when the stable cycle coalesces with a saddle cycle.

4.1. *Ansatz for moving solutions*

The governing equations for the infinite-N system are

$$\dot{\theta}_\alpha = E + \sin(\alpha - \theta_\alpha) + Kr\sin(\psi - \theta_\alpha), \quad \alpha \in [0, 2\pi]. \tag{4.1a}$$

$$re^{i\psi} = \frac{1}{2\pi}\int_0^{2\pi} e^{i\theta_\alpha}\, d\alpha \tag{4.1b}$$

$$\theta(\alpha + 2\pi, t) = \theta(\alpha, t) + 2\pi m, \quad \text{for integer } m. \tag{4.1c}$$

As always, we assume E, $K \geq 0$.

Numerical integration suggests that for $E > E_P(K)$ (4.1) has a unique, locally asymptotically stable moving solution with the following properties:

(i) All the θ_α execute identical motions but shifted in time and phase.

(ii) The coherence r and the collective velocity $v = \dot{\psi}$ are both independent of time.

(iii) The solution θ_α has degree $m = 0$:

$$\theta(\alpha, t) = \theta(\alpha + 2\pi, t)\ \forall \alpha, \forall t.$$

(iv) The moving solution is locally asymptotically stable for $E_P < E < E_T$ and globally asymptotically stable for $E > E_T$.

Property (i) above is the key to analyzing (4.1) for moving solutions. A more explicit statement of property (i) is that there is a 2π-periodic function ϕ: $\mathbb{R} \to \mathbb{R}$ such that (4.1) has a solution of the form

$$\theta_\alpha(t) = \psi(t) + \phi(\alpha - \psi(t)), \quad \alpha \in [0, 2\pi]. \tag{4.2}$$

Note that the same function ϕ appears in the *ansatz* for each θ_α, $\alpha \in [0, 2\pi]$; this is the sense in which all the θ_α execute identical motions. A similar *ansatz* has been used by other authors [13, 30, 37].

Fig. 9 illustrates a heuristic argument for the *ansatz* (4.2). The first term on the right side of (4.2) brings us into a reference frame moving with the average phase $\psi(t)$. In this frame at a fixed time, some θ_α are ahead of ψ and some are lagging it, depending on the location of their pinning phase α relative to ψ (fig. 9). As time evolves

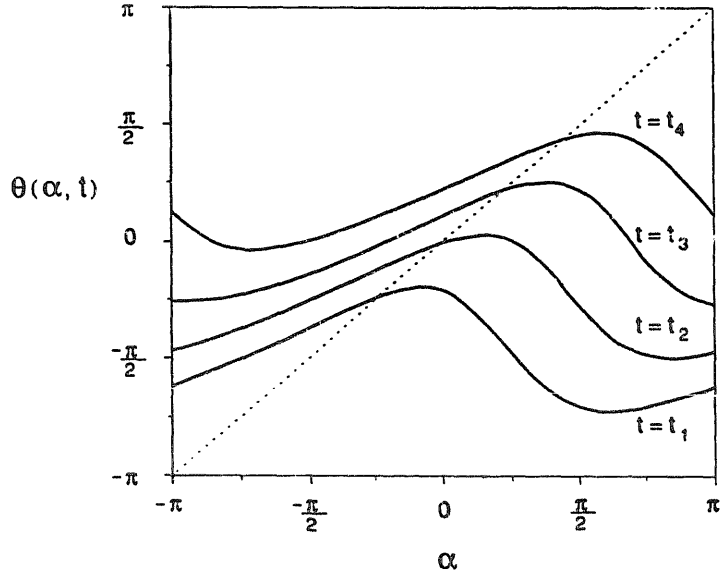

Fig. 9. Solutions $\theta(\alpha, t)$ of (4.1) for four equally spaced times, as obtained by numerical integration. The solutions at different times have identical shapes, but differ by a translation along the dashed line $\theta = \alpha$. Equivalently, one solution is related to another by a translation in both the θ and α directions. This observation motivates the *ansatz* (4.2).

$\psi(t)$ advances uniformly according to

$$\psi(t) = vt. \tag{4.3}$$

Meanwhile the position of the leading θ_α moves like a travelling wave in the α-direction; hence the wave variable $\alpha - \psi(t) = \alpha - vt$ appears as the argument of ϕ in (4.2). The function ϕ describes the shape of this travelling wave; in particular $\phi(\alpha) = \theta_\alpha(t = 0)$, since $\psi = 0$ when $t = 0$.

Now we use (4.2) to obtain a differential equation for the function ϕ. The argument of ϕ is the wave variable γ defined as

$$\begin{aligned}\gamma &= \alpha - \psi(t) \\ &= \alpha - vt.\end{aligned} \tag{4.4}$$

Differentiating (4.2) with respect to time we obtain

$$\begin{aligned}\dot{\theta}_\alpha &= \dot{\psi} + \phi'(\gamma)(-\dot{\psi}) \\ &= v(1 - \phi'(\gamma)),\end{aligned} \tag{4.5}$$

where prime denotes differentiation with respect to γ. Also

$$\begin{aligned}\sin(\alpha - \theta_\alpha) &= \sin(\alpha - [\psi + \phi]) \\ &= \sin(\gamma - \phi)\end{aligned} \tag{4.6}$$

and

$$\begin{aligned}Kr\sin(\psi - \theta_\alpha) &= Kr\sin(\psi - [\psi + \phi]) \\ &= -Kr\sin\phi.\end{aligned} \tag{4.7}$$

Hence (4.1a) becomes

$$v(1 - \phi') = E + \sin(\gamma - \phi) - Kr\sin\phi. \tag{4.8a}$$

The self-consistency condition (4.1b) may be rewritten as follows:

$$\begin{aligned}re^{i\psi} &= \frac{1}{2\pi}\int_0^{2\pi} e^{i\theta_\alpha}\,d\alpha \\ &= \frac{1}{2\pi}\int_0^{2\pi} e^{i\psi}e^{i\phi(\gamma)}\,d\gamma.\end{aligned}$$

Cancelling $e^{i\psi}$ and equating the real and imaginary parts of both sides of this equation, we obtain

$$r = \frac{1}{2\pi}\int_0^{2\pi}\cos\phi(\gamma)\,d\gamma, \tag{4.8b}$$

$$0 = \int_0^{2\pi}\sin\phi(\gamma)\,d\gamma, \tag{4.8c}$$

since r is assumed to be real and non-negative. The conditions (4.8b,c) may be expressed more compactly as $r = \langle\cos\phi\rangle$ and $0 = \langle\sin\phi\rangle$, where the averaging operator $\langle\cdot\rangle$ is defined by

$$\langle f\rangle = \frac{1}{2\pi}\int_0^{2\pi} f(\gamma)\,d\gamma.$$

The periodicity condition (4.1c) may be rewritten in terms of ϕ as $\phi(\gamma + 2\pi) = \phi(\gamma) + 2\pi m$. As mentioned above in property (iii), numerical simulations suggest that the moving solution has degree $m = 0$; hence we seek solutions satisfying

$$\phi(\gamma) = \phi(\gamma + 2\pi)\ \forall\,\gamma \in [0, 2\pi]. \tag{4.8d}$$

The problem posed by (4.8) is thus: Given $E \geq 0$, $K \geq 0$; find a 2π-periodic function ϕ and two numbers $r \geq 0$, $v \geq 0$ such that ϕ solves the differential equation (4.8a) and satisfies the side conditions $\langle\cos\phi\rangle = r$ and $\langle\sin\phi\rangle = 0$. This is a boundary value problem with three degrees of freedom and three constraints. For example, for fixed E and K we can choose values for $\phi(0)$, r, and v. Then we shoot forward to $\gamma = 2\pi$ by integrating (4.8a) with the chosen initial condition $\phi(0)$ and the chosen parameters r and v. This yields a function $\phi(\gamma)$ which depends on the chosen $\phi(0)$, r and v. If this function satisfies the side conditions $\langle\cos\phi\rangle = r$, $\langle\sin\phi\rangle = 0$, and $\phi(2\pi) =$

$\phi(0)$, then (4.8) has been solved. Otherwise we need to choose a different triple $(\phi(0), r, v)$ and continue the process.

From this argument it is not at all clear whether there will be *any* solutions to (4.8). Because we have as many degrees of freedom as we have constraints, there is reason to hope that solutions exist. In the next two sections we present formal asymptotic solutions of (4.8) for the cases $E \gg 1$ and $K \gg 1$.

(After this work was completed, Nancy Kopell pointed out to us that the implicit function theorem can be used to prove the existence of solutions to (4.8) for sufficiently large E. This argument will be presented elsewhere.)

4.2. *Perturbation theory*: $E \gg 1$

Numerical integration indicates that for $E \gg 1$ and $K = \mathcal{O}(1)$, there is a stable moving solution to (4.8) with

$$v \sim E, \quad r \sim 1 \quad \text{and} \quad \phi \ll 1. \tag{4.9}$$

That is, the high-field moving solution has all the θ_α nearly aligned with the average phase ψ.

These observations suggest that we seek a formal solution of (4.8) as a perturbation expansion in powers of

$$\epsilon = 1/E \ll 1. \tag{4.10}$$

Our strategy is to write expansions for r, v, and $\phi(\gamma)$ in powers of ϵ; then we solve the resulting differential equations at each order of ϵ, and use the conditions (4.8b, c, d) to determine the constants of integration and the unknown parameters in r and v. This procedure is carried out far enough to reveal the leading order dependence of ϕ, r, and v on ϵ and K.

One word about notation: for convenience, we often suppress the dependence on parameters in the expansions for v, r, and ϕ. The explicit dependences are

$$\begin{aligned} v &= v(\epsilon, K), \\ r &= r(\epsilon, K), \\ \phi &= \phi(\gamma, \epsilon, K). \end{aligned} \tag{4.11}$$

Using $\epsilon = 1/E$ we rewrite (4.8a) as

$$\epsilon v(1 - \phi') = 1 + \epsilon \sin(\gamma - \phi) - \epsilon K r \sin\phi. \tag{4.12}$$

As mentioned above, we expect $v \sim E$ and hence $\epsilon v \sim 1$ as $\epsilon \to 0$. Hence we expand ϵv as

$$\epsilon v = v_0 + \epsilon v_1 + \epsilon^2 v_2 + \cdots \tag{4.13}$$

with the expectation that $v_0 = 1$.

The expansions for $\phi(\gamma)$ and r are

$$\phi(\gamma) = \phi_0(\gamma) + \epsilon\phi_1(\gamma) + \epsilon^2\phi_2(\gamma) + \cdots, \tag{4.14}$$

$$r = r_0 + \epsilon r_1 + \epsilon^2 r_2 + \cdots. \tag{4.15}$$

In the appendix we carry out the analysis in detail. The results are:

$$\begin{aligned} \phi(\gamma) = \frac{1}{E}\cos\gamma + \frac{1}{E^2}\left(K\sin\gamma + \tfrac{1}{4}\sin 2\gamma\right) \\ + \frac{1}{E^3}\left(\left[\tfrac{1}{4} - K^2\right]\cos\gamma - \tfrac{3}{8}K\cos 2\gamma \right. \\ \left. - \tfrac{1}{12}\cos 3\gamma\right) + \mathcal{O}(E^{-4}), \end{aligned} \tag{4.16}$$

$$r = 1 - \frac{1}{4E^2} + \frac{1}{4E^4}\left(K^2 - \tfrac{1}{2}\right) + \mathcal{O}(E^{-5}), \tag{4.17}$$

$$v = E - \frac{1}{2E} + \frac{1}{2E^3}\left(K^2 - \tfrac{1}{8}\right) + \mathcal{O}(E^{-4}). \tag{4.18}$$

Fig. 10 shows that our third-order series solutions agree well with numerical solutions even when $E = \mathcal{O}(1)$. For $E \gg 1$ the series solution is indistinguishable from the numerical solution, and is therefore not shown.

4.3. *Perturbation theory*: $K \gg 1$

We now consider the strong-coupling limit $K \gg 1$ with $E = \mathcal{O}(1)$. The techniques are very

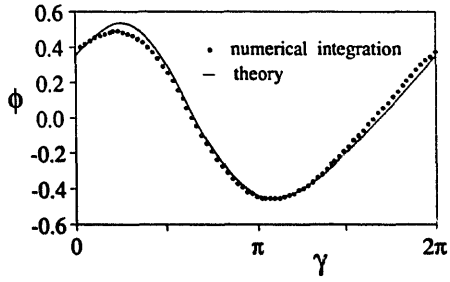

Fig. 10. The data points show the steady-state configuration $\phi(\gamma)$ obtained by numerical integration of (4.8) for $K = 1$ and $E = 2$. The perturbation theory result (4.16) is plotted as the continuous curve; it compares well with the numerical solution, even though E is far from the high-field limit $E \gg 1$ on which the perturbation theory is based.

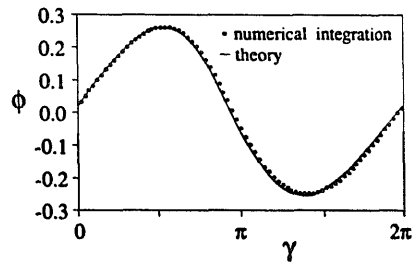

Fig. 11. The data points show the steady-state configuration $\phi(\gamma)$ obtained by numerical integration of (4.8) for $K = 4$ and $E = 0.5$. The perturbation theory result (4.21) is plotted as the continuous curve; it compares well with the numerical solution, even though K is far from the strong-coupling limit $K \gg 1$ on which the perturbation theory is based.

similar to those of section 4.2, but the analysis is slightly easier; at each order of perturbation theory, the next term in the unknown function ϕ is generated by differentiation rather than integration of previous terms.

The main results are asymptotic expressions for the configuration $\phi(\gamma)$, the coherence r, and the collective velocity v, expanded in powers of $1/K$. We find that for small E the velocity v is proportional to the applied field E. In particular, the depinning threshold E_T vanishes in this strong-coupling limit $K \gg 1$. The results of sections 2 and 3 prove the stronger result that $E_T(K) = 0$ for all $K > 2$. Fisher [12, 13] also found these results ($v \propto E$ and vanishing E_T in the strong-coupling limit) for a closely related mean-field model.

In this section, the small parameter ϵ is given by

$$\epsilon = 1/K.$$

Then (4.8a) becomes

$$v(1 - \phi') = E + \sin(\gamma - \phi) - \frac{1}{\epsilon} r \sin\phi. \tag{4.19}$$

We seek solutions of the form

$$\begin{aligned} \phi &= \phi_0 + \epsilon\phi_1 + \cdots, \\ r &= r_0 + \epsilon r_1 + \cdots, \\ v &= v_0 + \epsilon v_1 + \cdots \end{aligned} \tag{4.20}$$

subject to the conditions (4.8b, c, d).

The detailed calculations are carried out in the appendix. The results are:

$$\begin{aligned} \phi(\gamma) = {} & \frac{1}{K}\sin\gamma + \frac{1}{K^2}\left(E\cos\gamma - \tfrac{1}{2}\sin 2\gamma\right) \\ & + \frac{1}{K^3}\left(\left[\tfrac{1}{4} - E^2\right]\sin\gamma - \tfrac{3}{2}E\cos 2\gamma \right. \\ & \left. + \tfrac{1}{3}\sin 3\gamma\right) + \mathcal{O}\left(\frac{1}{K^4}\right). \end{aligned} \tag{4.21}$$

$$r = 1 - \frac{1}{4K^2} + \frac{1}{K^4}\left(\frac{E^2}{4} - \frac{11}{64}\right) + \mathcal{O}\left(\frac{1}{K^6}\right). \tag{4.22}$$

$$\frac{v}{E} = 1 - \frac{1}{2K^2} + \mathcal{O}\left(\frac{1}{K^4}\right). \tag{4.23}$$

Fig. 11 shows that the solution agrees well with numerical results even if K is not large.

4.4. *The pinning threshold* E_P

We now offer some conjectures about the bifurcation at $E = E_P(K)$. First consider the static case when $E = 0$, for which we have rigorous results. Fig. 3 indicates that the point $E = 0$, $K = K_c$ lies on the pinning threshold. As discussed in sections 2.1.3 and 2.1.4, for K slightly greater than K_c the system has a circle of saddle equilibrium points and a circle of stable equilibrium points in the full space of configurations (fig. 8). These circles are

parametrized by ψ. A jump bifurcation occurs at $K = K_c$ as the circle of saddle points coalesces with the circle of stable points. For $K < K_c$ the sinks and saddles have annihilated, leaving the incoherent pinned configuration $\theta(\alpha) = \alpha$ as the only attractor. These statements were proven in [28].

For $K > K_c$ and $E = 0$, the circle of saddle points and the circle of stable points are each neutrally stable to motions along the circle, as discussed in section 2.1.3. For $E = 0^+$, we conjecture that the circle of stable points loses this neutral stability and becomes a stable limit cycle. The circle of saddle points for $E = 0$ is expected to become a saddle cycle for $E > 1 - Kr$, as discussed in section 2.2.2.

Fig. 12 shows these limit cycles and their bifurcations in a schematic format analogous to fig. 8. Each of these cycles in configuration space represents a moving solution to (4.1). The motion along the cycles is expected to be uniform, because of the rotational symmetry in the problem.

Fig. 12 leads us to believe that *the pinning threshold $E_P(K)$ is defined by the condition that the stable cycle and the saddle cycle have coalesced.* As $E \to E_P(K)$ one of the Floquet multipliers (corresponding to perturbations transverse to the stable cycle and toward the saddle cycle) is expected to approach zero.

However the velocity *along* the cycles is not expected to approach zero as $E \to E_P(K)$. Thus we expect a genuine discontinuity in the velocity v at $E = E_P(K)$, as indicated in fig. 2(a). If correct, this discontinuity in v would be of theoretical interest because it distinguishes the repinning of this system from that of the hysteretic dc-driven Josephson junction and the damped pendulum driven by a constant torque. Daniel Fisher has pointed out to us that in these latter systems the analogue of the velocity tends to *zero continuously* (but with infinite derivatives of all orders) as $E \to E_P$, according to

$$v \propto \frac{1}{\ln(E - E_P)}. \tag{4.24}$$

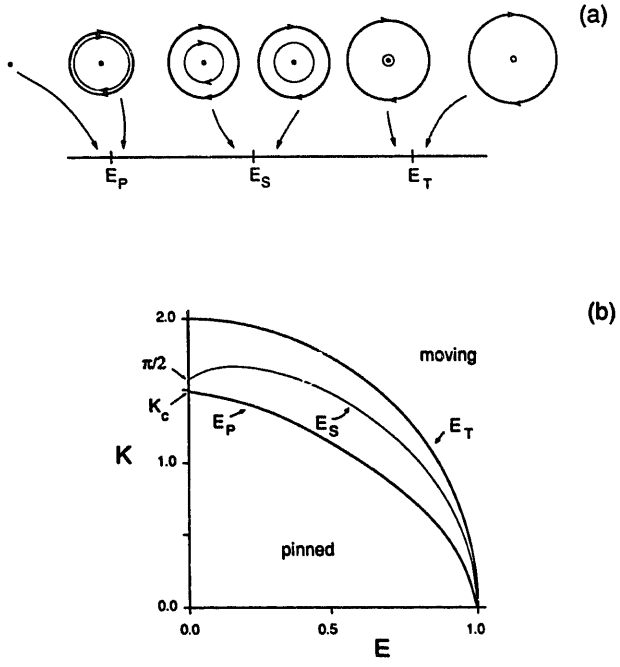

Fig. 12. (a) Schematic bifurcation diagram for steady-state solutions of (4.1) with $E > 0$. The coherence r and the average phase $\psi(t)$ of the solutions are plotted in polar coordinates. The origin corresponds to the pinned state $\theta_\alpha = \alpha + \sin^{-1} E$, which is locally stable for $E < E_T$. A saddle limit cycle (thin line) and a stable limit cycle (thick line) are born at large r when $E = E_P$. Motion along the saddle cycle stops at $E = E_S$, giving rise to a circle of saddle equilibrium points; the stopping threshold E_S is defined by the condition $E + Kr = 1$ given in (2.25). The circle of saddle points coalesces with the pinned state at $E = E_T$. At this coalescence the $r = 0$ pinned state becomes unstable. Above E_T the only attractor is the stable limit cycle corresponding to the coherent moving solution. (b) Stability diagram as in fig. 3, but with the stopping threshold E_S added. The points (K_S, E_S) on the stopping threshold are defined by the parametric equations $E_S = 1 - u$ and $K_S = u/r(u)$; the coherence $r(u)$ was obtained by numerical quadrature of the integral in (2.26).

For the Josephson junction, v and E correspond to the dc-voltage and the applied current, respectively; for the driven pendulum they represent the average velocity and the applied torque.

The bifurcation which leads to (4.24) has completely different phase space geometry from that in our system: The velocity dependence (4.24) occurs when a stable limit cycle passes near a saddle *point*, and motion on the cycle becomes extremely non-uniform and slow in the neighborhood of that point. We believe that in our system,

a discontinuity in the velocity occurs when a stable limit cycle collides with a saddle *cycle* (fig. 12). Motion along the cycle is expected to be uniform with velocity bounded away from zero even as $E \to E_p$.

5. Delayed switching

Thus far we have only been concerned with the steady-state behavior of (1.5). We now turn to an analysis of delayed switching, an interesting transient phenomenon seen when the coupling K and the applied field E are chosen just above the depinning threshold $E^2 + (K/2)^2 = 1$, and when the initial configuration is incoherent. Above threshold the only stable solutions have large coherence $r \approx 1$. Close to threshold, the evolution from an incoherent initial state to the coherent steady state will take much longer than the time scale on which a single, uncoupled phase would evolve.

There is a simple heuristic explanation for this delayed onset of coherence. Recall that for $E = 0$ the equation of motion is $\dot{\theta}_i = \sin(\alpha_i - \theta_i) + Kr \sin(\psi - \theta_i)$. Hence an initial configuration with $r \approx 0$ evolves as if the system were uncoupled. Thus an initially incoherent system will evolve towards the equilibrium $\theta_i = \alpha_i$, which is *stable* for the uncoupled system but which is *unstable* for the coupled system with K above threshold $K_T = 2$. After remaining in the vicinity of the unstable equilibrium $\theta_i = \alpha_i$ the system will slowly develop coherence and then depin suddenly once the coherence becomes appreciable.

Fig. 13 shows an example of this delayed onset of coherence beginning from a random initial configuration with $K = 2.001$ and $E = 0$, obtained by numerical integration of (1.2). This figure illustrates the rapid initial evolution towards the unstable equilibrium $\theta_i = \alpha_i$ followed by the slow development of coherence. Fig. 13(a) plots the time-evolution of the coherence r, showing that r stays small for about 20 time units and then grows rapidly, reaching a steady-state value of $r \approx 0.92$.

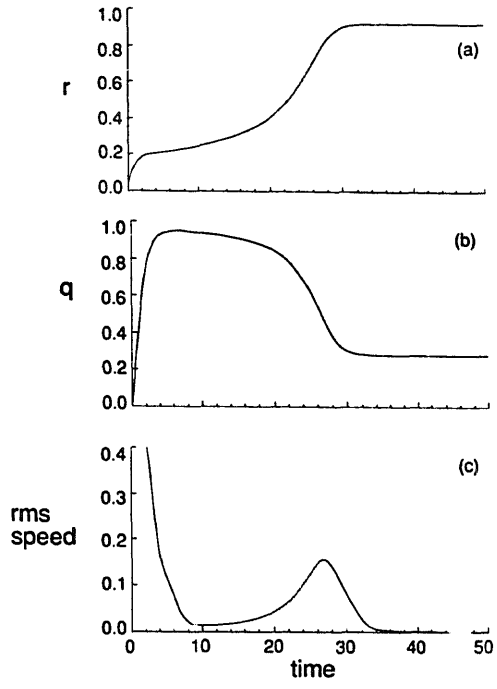

Fig. 13. Evolution of r, q and root-mean-square (rms) speed as the system evolves from incoherence to coherence. Eq. (1.2) with $K = 2.001$ and $E = 0$ was integrated numerically for $N = 300$ phases, starting from a random initial condition. The system rapidly approaches the pinned state $\theta_i = \alpha_i$, as shown by the large value of q after $t \approx 5$. Then the system slowly develops coherence between $t \approx 10$ and $t \approx 20$. A second peak in the rms speed occurs at $t \approx 26$ as the system leaves the neighborhood of the pinned state and rapidly switches to the coherent attractor. Compare fig. 4, which shows the same dynamics at the level of the individual phases.

A new order parameter q, defined as

$$q = \frac{1}{N} \sum_{i=1}^{N} \cos(\alpha_i - \theta_i),$$

characterizes how close the system is to the pinned configuration. Fig. 13(b) shows that q grows as the initially random phases flow towards the pinned configuration $\theta_i = \alpha_i$ and then decreases as the system leaves the pinned state towards the stable coherent state. Fig. 13(c) shows that the root-mean-square speed of the system has two peaks, one corresponding to the initial approach to the pinned state, and another corresponding to the later switch to the coherent attractor.

The choice $E = 0$ used above is special in the sense that the steady-state solution is static, but this does not affect the qualitative features of the delayed switching. Throughout this section we will concentrate on the case $E = 0$. The case $E > 0$, which is relevant to the delayed switching observed experimentally in some charge-density wave systems [21, 47], will be discussed in a subsequent paper.

In section 5.1, we present data from numerical simulations characterizing delayed switching for the case $E = 0$. In particular we study the dependence of the time delay τ on the proximity to threshold defined by $\kappa = K - K_T$. Section 5.2 presents an analytical expression for the delay τ in terms of κ and the initial coherence r_0. The results presented in section 5.2 are derived in section 5.3 using regular perturbation theory about the unstable equilibrium at $\theta_i = \alpha_i$. The analysis makes use of the fact that nearly all of the time delay occurs as the system is leaving this unstable equilibrium.

5.1. *Switching delay for $E = 0$: Numerical results*

Fig. 14 shows the evolution of the coherence r obtained from numerical integration of (1.2) for three values of coupling K near threshold. The switching delay τ increases as K nears the threshold value $K_T = 2$. Fig. 15 shows the dependence of τ on $\kappa = K - K_T$, where τ is defined by the condition that r becomes $\mathcal{O}(1)$. Over the regime of κ shown, the dependence is well approximated by a power law $\tau \propto \kappa^{-\beta}$, where $0.9 < \beta < 1$. The deviation from a strict $\beta = 1$ power law will be discussed in section 5.2.

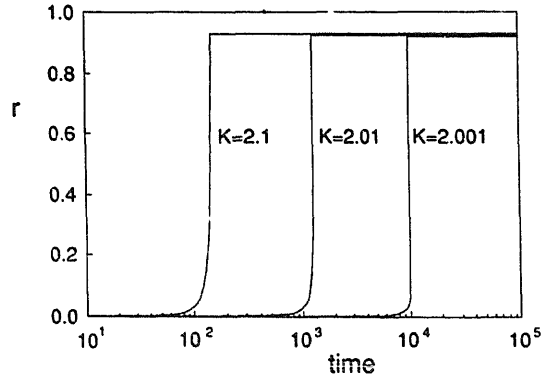

Fig. 14. Delayed onset of coherence for different values of K above the depinning threshold. Note that the time axis is logarithmic. Eq. (1.2) was integrated numerically for $N = 300$ phases, $E = 0$, and for the three values of K shown. All three integrations were started from the same initial condition, which was chosen near the pinned state according to $\theta_i = \alpha_i + \eta_i$, where the η_i were small random numbers of order $\mathcal{O}(10^{-2})$.

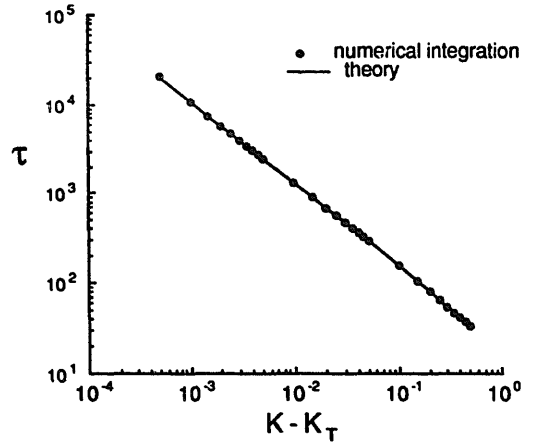

Fig. 15. Dependence of the switching delay τ on $K - K_T$, the distance from the depinning threshold. The data points are obtained by numerical integration of (1.2) as described in fig. 14. The initial condition for all the integrations had coherence $r_0 \approx 1.4 \times 10^{-2}$. The continuous curve shows the analytical result (5.3) for this value of r_0.

5.2. *Switching delay for $E = 0$: Analytical results*

As discussed above, an initially incoherent system first evolves toward the saddle equilibrium $\theta_i = \alpha_i$ and then departs along the unstable manifold. During this departure, the coherence r grows according to the evolution equation

$$\dot{r} = \left(\frac{K-2}{2}\right) r + \left(\frac{3-K}{2}\right) r^3 + \mathcal{O}(r^4), \qquad (5.1)$$

as derived in section 5.3. Eq. (5.1) implies that the coherence grows faster than exponentially for $2 < K < 3$. This superexponential growth becomes significant once r becomes large enough that the cubic term matches the linear term. Thus at

value of r given by

$$r^2 \approx \frac{K-2}{3-K} \tag{5.2}$$

the system evolves superexponentially and suddenly switches to the coherent state.

The condition (5.2) provides a natural definition of the time at which switching occurs. If the initial coherence satisfies $r_0^2 \ll (K-2)/(3-K)$, then the first term on the right side of (5.1) is initially dominant and the coherence grows according to $r(t) \approx r_0 e^{\kappa t/2}$. (Here t is measured from the time when the system first reaches the neighborhood of the pinned state.) Then the switching time τ is defined by the condition (5.2):

$$\frac{K-2}{3-K} \approx r_0^2 e^{\kappa\tau}.$$

For $\kappa = K-2 \ll 1$ this yields the switching delay

$$\tau \approx \frac{1}{\kappa} \ln\left(\frac{\kappa}{r_0^2}\right). \tag{5.3}$$

Fig. 15 shows that this theoretical value of the delay agrees well with the values obtained by numerical integration of (1.2). In general (5.3) is expected to hold for κ in the range $r_0^2 \ll \kappa \ll 1$.

A theory of delayed switching which neglected the cubic term in eq. (5.1) would yield $\tau \propto \kappa^{-\beta}$ with $\beta = 1$. Although (5.3) is dominated by the $1/\kappa$ term for $\kappa \ll 1$, the important logarithm term affects not only the magnitude of the delay but also its scaling with κ, giving an approximate value of β which is less than one. For the values of K and r_0 used in our numerical integration, both the numerical data and eq. (5.3) can be fit by an approximately power law scaling: $\tau \propto \kappa^{-\beta}$ with $\beta = 0.96$. This approximate power law was obtained for κ in the range $10^{-4} < \kappa < 10^{-1}$.

The cubic term in (5.1) is also important for $r_0^2 > (K-2)/(3-K)$, in which case the cubic term dominates the linear term from the start. In particular, at threshold the coherence grows non-exponentially according to

$$r(t) \approx \left(r_0^{-2} - t\right)^{-1/2} \quad [\text{for } K = K_T = 2] \tag{5.4}$$

before r saturates near 1. Eq. (5.4) shows that the timescale at threshold is $\mathcal{O}(r_0^{-2})$, which is much longer than τ in (5.3) for small r_0. On the other hand, (5.4) also shows that the delay before r becomes $\mathcal{O}(1)$ does not diverge as $K \to K_T$.

5.3. *Evolution equation for coherence*

We now derive the evolution equation (5.1). This equation describes the growth of coherence for a system evolving along the unstable manifold of the saddle pinned state. In the infinite-N limit the dynamics of the phases at $E = 0$ are governed by

$$\dot{\theta}_\alpha = \sin(\alpha - \theta_\alpha) + u \sin(\psi - \theta_\alpha). \tag{5.5}$$

We must now find a self-consistent solution for u, as before, but with the added complication that $u(t)$ evolves in time.

In numerical solutions of (5.5) the average phase ψ remains essentially constant as the phases θ_α evolve. We make use of this observation by seeking solutions of (5.5) of the form

$$\theta_\alpha = \psi + \phi(\alpha - \psi, u) \tag{5.6}$$

and insist that

$$\dot{\psi} = 0$$

throughout the evolution. This *ansatz* (5.6) is closely related to that used in section 4.1; the difference is that here u depends on time and ψ is time-independent. This *ansatz* is valid after the system has completed its initial rapid evolution toward the pinned state and has begun to depart very slowly from the saddle pinned state along its unstable manifold.

Substituting (5.6) into (5.5) yields

$$\frac{\partial \phi}{\partial u}\dot{u} = \sin(\gamma - \phi) - u \sin\phi, \tag{5.7}$$

where $\gamma \equiv \alpha - \psi$. The self-consistency equation for u is

$$u = K\langle \cos\phi \rangle, \tag{5.8}$$

where the brackets denote the average over one cycle of γ, as in (4.8b).

Two symmetries of (5.7) restrict the form of its solutions: First, (5.7) is invariant under the transformation

$$\gamma \to -\gamma,$$
$$\phi \to -\phi$$

and therefore its solutions must satisfy

$$\phi(u,\gamma) = -\phi(u,-\gamma). \tag{5.9}$$

Second, (5.7) is invariant under the transformation

$$\gamma \to \gamma + \pi,$$
$$\phi \to \phi + \pi,$$
$$u \to -u$$

and therefore its solutions must satisfy

$$\pi + \phi(u,\gamma) = \phi(-u, \pi + \gamma). \tag{5.10}$$

We assume that close to the unstable equilibrium $\phi(u,\gamma) = \gamma$, we can express $\phi - \gamma$ as a Fourier series in γ with small amplitudes $a_k(u)$ which grow as the system leaves the unstable equilibrium and develops coherence. The symmetries (5.9) and (5.10) require that such solutions be of the form

$$\phi(u,\gamma) = \gamma - \sum_{k=1}^{\infty} a_k(u) \sin k\gamma, \tag{5.11}$$

where the amplitudes $a_k(u)$ satisfy

$$a_k(u) = \begin{cases} a_k(-u), & k \text{ even}, \\ -a_k(-u), & k \text{ odd}. \end{cases} \tag{5.12}$$

The leading order term in (5.11) appeared already in (2.35) for the unstable mode about the pinned state $\phi(u,\gamma) = \gamma$. Eq. (5.11) enables us to extend the earlier linear stability analysis to include nonlinear terms in the small parameter u.

Now we substitute (5.11) into (5.7), expand both sides in Fourier series, and collect the resulting terms in $\sin k\gamma$ for each k. Matching the coefficients of $\sin k\gamma$ on both sides of (5.7) yields a set of coupled ordinary differential equations describing the evolution of the amplitudes $a_k(u)$. For our purposes it is sufficient to study the evolution of the first two amplitudes, $a_k(u)$ for $k = 1, 2$. Because both u and the $a_k(u)$ are small near the unstable equilibrium $\phi(u,\gamma) = \gamma$, we assume a power series form for the $a_k(u)$. The most general series for these amplitudes which satisfy (5.12) and which vanish at $u = 0$ are

$$a_1(u) = b_1 u + b_3 u^3 + \mathcal{O}(u^5), \tag{5.13a}$$

$$a_2(u) = c_2 u^2 + \mathcal{O}(u^4). \tag{5.13b}$$

Substituting (5.11) and (5.13) into (5.7) eventually yields

$$-\dot{u}\frac{da_1}{du} = (b_1 - 1)u + \left(b_3 - \frac{b_1^3}{8} + \frac{3b_1^2}{8} + \frac{c_2}{2}\right)u^3 + \mathcal{O}(u^4), \tag{5.14a}$$

$$-\dot{u}\frac{da_2}{du} = \left(c_2 + \frac{b_1}{2}\right)u + \mathcal{O}(u^4). \tag{5.14b}$$

The unknown constants b_1, b_3, and c_2 are determined by the self-consistency condition (5.8) and by the requirement that there be a unique evolution equation for u, that is (5.14a) and (5.14b) must give the same differential equation for $\dot{u}$. These conditions can be shown to imply

$$b_1 = \frac{2}{K}, \quad c_2 = \frac{1}{(1-K)K},$$

$$b_3 = \frac{1}{(1-K)K^3}.$$

After substituting these values into (5.14a) we

obtain the evolution equation for u:

$$\dot{u} = \left(\frac{K-2}{2}\right)u + \left(\frac{3-K}{2K^2}\right)u^3 + \mathcal{O}(u^4).$$

Finally, substituting $u = Kr$ gives the equation for the evolution of coherence r discussed in section 5.2:

$$\dot{r} = \left(\frac{K-2}{2}\right)r + \left(\frac{3-K}{2}\right)r^3 + \mathcal{O}(r^4).$$

6. Concluding remarks and open problems

In this paper we have studied the dynamics of a system of many oscillators with random pinning and periodic coupling. The goal has been to present a case study of collective nonlinear dynamics in a model which is simple enough to yield to analysis and yet rich enough to possess interesting dynamics. To facilitate the analysis, we have made two assumptions familiar from statistical mechanics: that the coupling between oscillators has infinite range and that the system is infinitely large.

Most previous studies of the collective dynamics of coupled oscillators have been concerned with the mutual synchronization of oscillators whose intrinsic frequencies are randomly distributed [1, 7–9, 11, 22–25, 31, 32, 34, 38, 39, 43, 44] or noisy [5, 6, 33, 35, 36, 45, 46]. These studies show that mutual synchronization is remarkably similar to the second-order phase transitions seen in equilibrium statistical mechanics [27]. That is, the order parameter characterizing synchronization grows continuously from zero as the coupling exceeds a critical value.

In contrast, the collective dynamics of the system studied in this paper is more suggestive of a first-order phase transition [3]. The transition from a disordered and static state to an ordered and moving state occurs discontinuously, with hysteresis in both the coupling strength and the driving field. The onset of order from an initially incoherent state also shows an interesting and novel time delay near threshold. The first-order character of the depinning transition is directly attributable to the periodic coupling $\sin(\theta_i - \theta_j)$ in (1.2). Alternate models with linear coupling, corresponding to an elastic interaction between phases [2, 12, 13, 37, 42] do not show switching, hysteresis or delayed onset of order.

There are several open mathematical problems concerning the dynamical system (1.5): (1) Prove rigorously that there is a unique, locally stable, steady-state moving solution for each E and K with $E > E_p(K)$ and (2) prove that this solution disappears at $E = E_p(K)$ via coalescence with an unstable solution. (3) Find a closed form expression for the pinning threshold $E_p(K)$. (4) Characterize the basins of attraction for the incoherent pinned solution and the coherent moving solution in the bistable regime $E_p < E < E_T$. (Preliminary numerical work suggests that the basins are characterized only by the coherence of the initial configuration.)

Before the model can be applied to charge-density waves or other real physical systems, it needs to be extended in various ways. Most importantly, it is not known which aspects of the mean-field dynamics will survive with short-range coupling in finite dimension. Numerically we find that in dimension $d = 3$ the discontinuity at depinning remains but is weakened. We do not know if switching in $d = 3$ is a finite size effect of the numerics: simulations with various N show that the discontinuity decreases as the system size is increased. It is also unknown whether there is an upper critical dimension [12, 13, 27, 30] above which the dynamics agree with those found here in mean-field theory. The effects of temperature, distributed pinning strengths and distributed field strengths also deserve future study.

Appendix: Perturbation theory calculations

This appendix gives the perturbation calculations needed in sections 4.2 and 4.3.

A.1. *Perturbation theory for $E \gg 1$*

We begin by substituting (4.13)–(4.15) into (4.12). At $\mathcal{O}(1)$ this yields

$$v_0(1-\phi_0') = 1,$$

which has the solution

$$\phi_0(\gamma) = \left(\frac{v_0-1}{v_0}\right)\gamma + C_0, \tag{A.1}$$

where C_0 is a constant of integration. From (4.8d), ϕ_0 must be 2π-periodic and therefore $\phi_0(2\pi) = \phi_0(0)$. Hence the coefficient of γ in (A.1) vanishes, which implies

$$v_0 = 1$$

as expected. Thus $\phi_0(\gamma) = C_0$. From (4.8c) $\langle \sin\phi_0\rangle = 0$ and so $\phi_0 = n\pi$ for integer n. Since $r = \langle\cos\phi\rangle$ is non-negative by assumption, n must be even. Without loss of generality we take the solution

$$\phi_0(\gamma) \equiv 0. \tag{A.2}$$

$\mathcal{O}(\epsilon)$ *equations*: The differential equation (4.12) at $\mathcal{O}(\epsilon)$ is

$$v_1 - \phi_1' = \sin\gamma,$$

which has a solution

$$\phi_1(\gamma) = v_1\gamma + \cos\gamma + C_1. \tag{A.3}$$

Since $\phi_1(0) = \phi_1(2\pi)$ we obtain

$$v_1 = 0. \tag{A.4}$$

To evaluate C_1 we expand the condition (4.8c):

$$\begin{aligned} 0 &= \langle\sin\phi\rangle \\ &= \left\langle \phi - \frac{\phi^3}{3!} + \frac{\phi^5}{5!} \cdots \right\rangle \\ &= \epsilon\langle\phi_1\rangle + \epsilon^2\langle\phi_2\rangle + \epsilon^3\left\langle \phi_3 - \frac{\phi_1^3}{3!}\right\rangle + \mathcal{O}(\epsilon^4), \end{aligned}$$

where we have used the fact that $\phi_0 \equiv 0$. Thus

$$\langle\phi_1\rangle = 0, \tag{A.5a}$$

$$\langle\phi_2\rangle = 0, \tag{A.5b}$$

$$\left\langle \phi_3 - \frac{\phi_1^3}{6}\right\rangle = 0. \tag{A.5c}$$

Eqs. (A.3) and (A.4) imply $\langle\phi_1\rangle = \langle\cos\gamma\rangle + C_1 = C_1$ and therefore (A.5a) yields

$$C_1 = 0,$$

$$\phi_1(\gamma) = \cos\gamma. \tag{A.6}$$

Combining (A.2) and (A.6) gives the first four terms in the expansion for r:

$$\begin{aligned} r &= \langle\cos\phi\rangle \\ &= \left\langle 1 - \frac{\phi^2}{2!} + \frac{\phi^4}{4!} \cdots \right\rangle \\ &= 1 - \frac{\epsilon^2}{2}\langle\cos^2\gamma\rangle + \mathcal{O}(\epsilon^4) \\ &= 1 - \frac{\epsilon^2}{4} + \mathcal{O}(\epsilon^4). \end{aligned}$$

Hence

$$r_0 = 1, \quad r_1 = 0, \quad r_2 = -\tfrac{1}{4}, \quad r_3 = 0.$$

$\mathcal{O}(\epsilon^2)$ *equations*: The differential equation (4.12) at $\mathcal{O}(\epsilon^2)$ is

$$v_2 - v_1\phi_1' - \phi_2' = -Kr_0\phi_1 - \phi_1\cos\gamma. \tag{A.7}$$

Using $v_1 = 0$, $r_0 = 1$, and $\phi_1 = \cos\gamma$, (A.7) simplifies to

$$\begin{aligned} \phi_2' &= v_2 + K\cos\gamma + \cos^2\gamma \\ &= \left(v_2 + \tfrac{1}{2}\right) + K\cos\gamma + \tfrac{1}{2}\cos^2\gamma. \end{aligned} \tag{A.8}$$

Eq. (A.8) has the solution

$$\phi_2(\gamma) = \left(v_2 + \tfrac{1}{2}\right)\gamma + K\sin\gamma + \tfrac{1}{4}\sin 2\gamma + C_2.$$

As argued previously, the coefficient of γ vanishes

because $\phi_2(2\pi) = \phi_2(0)$. Hence

$$v_2 = -\tfrac{1}{2}.$$

Moreover $C_2 = 0$ because of the condition (A.5b). The resulting expression for ϕ_2 is

$$\phi_2(\gamma) = K\sin\gamma + \tfrac{1}{4}\sin 2\gamma.$$

$\mathcal{O}(\epsilon^3)$: We omit the details. The main results are

$$v_3 = 0,$$
$$\phi_3(\gamma) = \left(\tfrac{1}{4} - K^2\right)\cos\gamma - \tfrac{3}{8}K\cos 2\gamma - \tfrac{1}{12}\cos 3\gamma.$$

These results allow us to see the leading order dependence of r and v on K, which enters only now. We compute r as follows:

$$\begin{aligned} r &= \langle\cos\phi\rangle \\ &= 1 - \frac{\epsilon^2}{2}\langle\phi_1^2\rangle - \epsilon^3\langle\phi_1\phi_2\rangle \\ &\quad + \epsilon^4\left\langle \frac{\phi_1^4}{4!} - \frac{\phi_2^2}{2!} - \phi_1\phi_3 \right\rangle + \mathcal{O}(\epsilon^5) \\ &= 1 - \frac{\epsilon^2}{4} + \frac{\epsilon^4}{4}\left(K^2 - \tfrac{1}{2}\right) + \mathcal{O}(\epsilon^5). \end{aligned}$$

One might think it necessary to go to $\mathcal{O}(\epsilon^4)$ to obtain an expression for v_4. An earlier method uses the identity

$$v = E + \langle\sin(\gamma - \phi)\rangle \tag{A.9}$$

obtained by averaging (4.8a) and using the facts that $\langle\sin\phi\rangle = 0$ and $\langle\phi'\rangle = [\phi(2\pi) - \phi(0)]/2\pi = 0$. The term $\langle\sin(\gamma - \phi)\rangle$ can be computed to $\mathcal{O}(\epsilon^3)$ by expanding $\sin\phi$ and $\cos\phi$ to $\mathcal{O}(\epsilon^3)$ and using the trigonometric identity for $\sin(\gamma - \phi)$. The result is

$$\langle\sin(\gamma - \phi)\rangle = -\tfrac{1}{2}\epsilon + \tfrac{1}{2}\epsilon^3\left(K^2 - \tfrac{1}{8}\right) + \mathcal{O}(\epsilon^4).$$

Therefore

$$v_4 = \tfrac{1}{2}\left(K^2 - \tfrac{1}{8}\right).$$

These results are summarized in section 4.2.

A.2. *Perturbation theory for $K \gg 1$*

Now we substitute (4.20) into (4.19) and match terms at each power of $\epsilon = 1/K$. The $\mathcal{O}(1/\epsilon)$ condition requires $r_0\sin\phi_0 = 0$. Hence, from (4.8c), $\sin\phi_0 = 0$. Since we are looking for solutions with $r > 0$, we find $\phi_0 = 2\pi n$ for integer n, and we choose

$$\phi_0 = 0$$

without loss of generality. Hence $r = \langle\cos\phi\rangle = 1 - (\epsilon^2/2)\langle\phi_1^2\rangle + \mathcal{O}(\epsilon^3)$, and (4.19) becomes

$$\begin{aligned} (v_0 + \epsilon v_1)(1 - \epsilon\phi_1') &= E + \sin(\gamma - \epsilon\phi_1) \\ &\quad - \frac{1}{\epsilon}\sin\left(\epsilon\phi_1 + \epsilon^2\phi_2\right) + \mathcal{O}(\epsilon^2). \end{aligned} \tag{A.10}$$

$\mathcal{O}(1)$ *equations*: The $\mathcal{O}(1)$ equation in (A.10) is $v_0 = E + \sin\gamma - \phi_1$. Hence

$$\phi_1 = E - v_0 + \sin\gamma. \tag{A.11}$$

The condition $\langle\sin\phi\rangle = 0$ implies

$$\langle\phi_1\rangle = \langle\phi_2\rangle = 0,$$

which applied to (A.11) yields

$$v_0 = E,$$
$$\phi_1(\gamma) = \sin\gamma. \tag{A.12}$$

$\mathcal{O}(\epsilon)$ *equations*: The $\mathcal{O}(\epsilon)$ equation in (A.10) is $v_1 - v_0\phi_1' = -\phi_1\cos\gamma - \phi_2$ or

$$\phi_2 = -\phi_1\cos\gamma - v_1 - E\phi_1'.$$

Note that the unknown function ϕ_2 is obtained from the previously found ϕ_1 by differentiation and substitution, but not integration. This occurs at all orders of perturbation theory. Here it yields

$$\phi_2 = -v_1 + E\cos\gamma - \sin\gamma\cos\gamma$$

and since $\langle \phi_2 \rangle = 0$,

$$v_1 = 0,$$

$$\phi_2(\gamma) = E\cos\gamma - \sin\gamma\cos\gamma$$
$$= E\cos\gamma - \tfrac{1}{2}\sin 2\gamma. \qquad \text{(A.13)}$$

To find v_2, we use the identity (A.9) as above. After substituting (A.12) and (A.13) into $\langle \sin(\gamma - \phi) \rangle = \langle \sin(\gamma - \epsilon\phi_1 - \epsilon^2\phi_2) \rangle + \mathcal{O}(\epsilon^3)$ and computing some integrals, we find $v_2 = -\frac{1}{2}E$. Thus

$$v = E - \tfrac{1}{2}\epsilon^2 E + \mathcal{O}(\epsilon^3).$$

Continuing in this way, we obtain higher order terms in ϕ, r, and v. These calculations are summarized in section 4.3.

Acknowledgements

We thank Nancy Kopell, Peter Littlewood, and Mark Sherwin for informative discussions, and Tom Orowan for preparing the manuscript. The research of SHS was supported by an NSF Postdoctoral Fellowship, Grant DMS-8605761. CMM acknowledges support as an AT&T Bell Laboratories Scholar. This research was supported in part by ONR Contract N00014-84-K-0465.

References

[1] Y. Aizawa, Prog. Theor. Phys. 56 (1976) 703.
[2] P. Alstrom and R.K. Ritala, Phys. Rev. A 35 (1987) 300.
[3] K. Binder, Rep. Prog. Phys. 50 (1987) 783.
[4] A.R. Bishop, G. Grüner and B. Nicolaenko, eds., Spatio-Temporal Coherence and Chaos in Physical Systems (North-Holland, Amsterdam, 1986).
[5] L.L. Bonilla, Phys. Rev. Lett. 60 (1988) 1398.
[6] L.L. Bonilla, J.M. Casado and M. Morillo, J. Stat. Phys. 48 (1987) 571.
[7] H. Daido, Prog. Theor. Phys. 75 (1986) 1460.
[8] H. Daido, J. Phys. A: Math. Gen. 20 (1987) L629.
[9] H. Daido, Phys. Rev. Lett. 61 (1988) 231.
[10] J. Dumas, C. Schlenker, J. Marcus and R. Buder, Phys. Rev. Lett. 50 (1983) 757.
[11] G.B. Ermentrout, J. Math. Biol. 22 (1985) 1.
[12] D.S. Fisher, Phys. Rev. Lett. 50 (1983) 1486.
[13] D.S. Fisher, Phys. Rev. B 31 (1985) 1396.
[14] H. Fukuyama and P.A. Lee, Phys. Rev. B 17 (1978) 535.
[15] G. Grüner and A. Zettl, Phys. Rep. 119 (1985) 117.
[16] R.P. Hall, M.F. Hundley and A. Zettl, Physica B143 (1986) 152.
[17] R.P. Hall, M.F. Hundley and A. Zettl, Phys. Rev. Lett. 56 (1986) 2399.
[18] M.F. Hundley and A. Zettl, Phys. Rev. B 37 (1988) 8817.
[19] G. Hutiray and J. Solyom, eds., Charge Density Waves in Solids, Lecture Notes in Physics 217 (Springer, Berlin, 1985).
[20] M. Inui, R.P. Hall, S. Doniach and A. Zettl, Phys. Rev. B 38 (1988) 13047.
[21] G. Kriza, A. Janoczy and G. Mihaly, in ref. [19], p. 426.
[22] Y. Kuramoto, Lecture Notes in Physics 39 (Springer, New York, 1975), p. 420.
[23] Y. Kuramoto, Chemical Oscillations, Waves and Turbulence (Springer, Berlin, 1984).
[24] Y. Kuramoto, Prog. Theor. Phys. Suppl. 79 (1984) 223.
[25] Y. Kuramoto and I. Nishikawa, J. Stat. Phys. 49 (1987) 569.
[26] P.A. Lee and T.M. Rice, Phys. Rev. B 19 (1979) 3970.
[27] S.K. Ma, Modern Theory of Critical Phenomena (Benjamin, New York, 1976).
[28] R.E. Mirollo and S.H. Strogatz, SIAM J. Appl. Math., in press.
[29] H. Mutka, S. Bouffard, J. Dumas and C. Schlenker, J. Physique. Lett. 45 (1984) L729.
[30] R.K. Ritala and J.A. Hertz, Phys. Scripta 34 (1986) 264.
[31] H. Sakaguchi, Prog. Theor. Phys. 79 (1988) 39.
[32] H. Sakaguchi, S. Shinomoto and Y. Kuramoto, Prog. Theor. Phys. 77 (1987) 1005.
[33] H. Sakaguchi, S. Shinomoto and Y. Kuramoto, Prog. Theor. Phys. 79 (1988) 600.
[34] H. Sakaguchi, S. Shinomoto and Y. Kuramoto, Prog. Theor. Phys. 79 (1988) 1069.
[35] M. Shiino, Phys. Lett. A 111 (1985) 396.
[36] S. Shinomoto and Y. Kuramoto, Prog. Theor. Phys. 75 (1986) 1105.
[37] L. Sneddon, Phys. Rev. B 30 (1984) 2974.
[38] S.H. Strogatz and R.E. Mirollo, Physica D 31 (1988) 143.
[39] S.H. Strogatz and R.E. Mirollo, J. Phys. A: Math. Gen. 21 (1988) L699.
[40] S.H. Strogatz, C.M. Marcus, R.M. Westervelt and R.E. Mirollo, Phys. Rev. Lett. 61 (1988) 2380.
[41] K. Tsutsumi, Physica B 143 (1986) 129.
[42] P.F. Tua and A. Zawadowski, Solid State Commun. 49 (1984) 19.
[43] A.T. Winfree, J. Theor. Biol. 16 (1967) 15.
[44] A.T. Winfree, The Geometry of Biological Time (Springer, New York, 1980).
[45] Y. Yamaguchi and H. Shimizu, Physica D 11 (1984) 212.
[46] Y. Yamaguchi, H. Kometani and H. Shimizu, J. Stat. Phys. 26 (1981) 719.
[47] A. Zettl and G. Grüner, Phys. Rev. B 26 (1982) 2298.